Ecological Archives **M074-011-A1 through A8**

Mark W. Denny, Brian Helmuth, George H. Leonard,

Christopher D. G. Harley, Luke J. H. Hunt, and Elizabeth K. Nelson

Appendix A. A Brief Primer on Spectral Analysis

Consider the hypothetical variable $y(x)$ depicted in Figure 1B. The location, x, along a particular spatial path is shown on the abscissa and the magnitude of the variable is shown on the ordinate. For example, if we moved a thermometer along a horizontal path through the intertidal zone and continuously measured both x, the total distance traveled, and y, the temperature of the rock surface, a graph similar to Fig. 1B would likely result.

The fluctuation in y is traditionally measured by its variance. In practice, y is sampled at a discrete set of locations, and the sample variance is calculated as

$$\sigma^2(y) = \frac{1}{n-1}\sum_{j=1}^{n}[y(x_j) - \mu_y]^2 \,. \qquad \text{(A1)}$$

Here, $y(x_j)$ is the magnitude of the function at the jth location, n is the total number of samples, and μ_y is the mean of the sampled values.

The variance describes the overall amount of fluctuation in a variable, but it does not describe how this fluctuation is divided among measurement scales. It is evident from Fig. 1B that in this particular case y tends to vary periodically along its path of measurement. This periodicity is

not perfect (e.g., sometimes there is a valley in y where a peak would be expected), but a dominant spatial pattern can be discerned. What is the scale of this pattern, and how can we calculate it?

A classic theorem (due to J. B. J. Fourier, 1768 - 1830) tells us that the spatial variation in y as a function of x can be quantified through the following procedure. The total length of our measured path, x_{max}, defines the largest scale about which we have any data (the extent of the data). Note that if all n samples are spaced Δx apart, the total length over which we have measured y is x_{max}:

$$x_{max} = (n-1)\Delta x . \qquad \text{(A2)}$$

Traditionally this extent is expressed not as x_{max} itself, but rather as the *fundamental spatial frequency*, f_f:

$$f_f = \frac{1}{x_{max}} . \qquad \text{(A3)}$$

A low spatial frequency corresponds to a large spatial extent, a high spatial frequency corresponds to a small spatial extent. Spatial frequency has units of m^{-1}.

Given the fundamental spatial frequency (which is set by the total path length), we describe the variation in y at a series of additional frequencies, f_i, each a harmonic of the fundamental. In other words, we examine spatial frequencies

$$f_i = if_f , \qquad \text{(A4)}$$

where i is an integer greater than 0.

At any given point x, the magnitude of y is:

$$y(x) = \sum_{i=1}^{g} b_i \sin(2\pi i f_f x + \varphi_i). \qquad \text{(A5)}$$

This is one form of the classic Fourier series (Bendat and Piersol 1986). In essence, we sum a series of harmonic sinusoidal waves (each with its own particular amplitude, b_i, and phase, ϕ_i) to

approximate the overall pattern of variation in y. This process is shown in Fig. 1C-L. The ten waves shown there (each a harmonic of the fundamental) sum to the overall waveform plotted in Figure 1B. Note that each harmonic has an integral number of wave lengths in the interval x_{max}. For simplicity in this example we set x_{max} to 1. Note that the third, seventh, and tenth harmonics of the fundamental have the largest amplitudes.

Having expressed the function $y(x)$ as the sum of a series of sine waves, we can now use the amplitude of each of these waves to calculate what fraction of the overall variance in y is associated with each of the spatial scales described by the harmonics of the fundamental spatial frequency. The details of the calculation need not concern us here (see Bendat and Piersol 1986); it is the end result that matters. The scale-specific (= frequency-specific) contribution to the overall variance in y is quantified by the *autospectral density function*, $S(f)$. If a large fraction of the overall variance in y occurs with a periodicity that falls in a particular small range in spatial frequencies, the S for that frequency range is large. Conversely, if little of the overall variation in y corresponds to a particular spatial frequency, the S for that frequency is small. The pattern of variation among frequencies is the *autospectrum* shown in Figure 2A, in this case for the process shown in Fig. 1B. Note that there are peaks in this autospectrum at the third, seventh, and tenth harmonics of the fundamental frequency, corresponding to those harmonics that have large amplitudes (Fig. 1C-L).

It is important to note several properties of the autospectrum. First, there is an upper limit, $i = g$, to the harmonic of f_f at which we can discern any variation in the process y, and this limit is set by the spacing, Δx, between our samples. If y varies at a scale smaller than $2\Delta x$, this variation cannot be reliably measured directly by our technique. The spatial frequency corresponding to a scale of $2\Delta x$ (known as the Nyquist frequency, f_g) is equal to $1/(2\Delta x)$. Working through the algebra, we find that $g = (n\text{-}1)/2$. The Nyquist frequency is equivalent to the lower limit of the spatial detail

we can discern (the grain of our measurements). Note that variation at frequencies above the Nyquist frequency is not excluded from our measurements. Instead, through a process known as *aliasing*, high frequency fluctuations appear in the form of spurious, "scrambled" variation at frequencies below the Nyquist frequency (see, for example, Press et al. 1992), and can thereby potentially affect our measurements.

Second, the integral of $S(f)$ across a particular range of frequencies is equal to the variance associated with those frequencies:

$$\text{variance in the frequency range } f_a \text{ to } f_b = \int_{f_a}^{f_b} S(f)df \ . \qquad \text{(A6)}$$

This is the basis for calculating the variance scale (Eqs. 7, B10) and for the calculations shown in Fig. 9. By extension, the integral of $S(f)$ between the fundamental and Nyquist frequencies is equal to the overall measurable variance in y:

$$\sigma^2(y) = \int_{f_f}^{f_g} S(f)df \ . \qquad \text{(A7)}$$

In other words, the total area under the autospectrum is equal to the overall variance.

Third, the units of $S(f)$ take into account the units of both y and x. For example, in the case described here y is measured in ^{o}C and x is measured in meters (so that spatial frequency has units of m^{-1}). The variance in temperature, σ^2 (the area under the curve), has units $^{o}C^2$. As a result, S must have the units $^{o}C^2m$.

Because the spectrum is calculated only for harmonics of the fundamental frequency (and are therefore orthogonal [see Priestley 1981]), the individual spectral estimates are independent. In other words, the spectrum calculated as described above provides the minimum number of sinusoidal waves required to exactly reproduce the sample data.

It is common that the magnitude of individual points in the autospectrum varies across a large range. When this is true, the fine structure of the spectrum may be dwarfed by the major peaks, and can thereby escape notice. As a remedy, spectra are often plotted on log-log axes, and this convention is used here in Appendix E. Note that areas under spectra can be visually distorted by the log transformation.

We have seen here that if a variable is characterized by periodic fluctuation at one particular spatial scale, this tendency will be exposed by the existence of a peak in the autospectrum. This does not imply, however, that all variables are periodic, nor that all periodic variables are characterized by single spectral peaks. A pertinent example is shown in Fig. A1. Here the data are clearly periodic (Fig. A1A), but not sinusoidal: in this case, all negative values of a sine wave have been set to zero, while the positive values are unchanged. The hypothetical variable shown here is very similar to measurements of environmental light intensity in which it is uniformly dark at night, but solar irradiance varies approximately sinusoidally throughout the day (Fig. E1). The spectrum of this process (Figs. A1B and C) is characterized by a series of peaks. The peak with the lowest spatial frequency corresponds to the overall periodicity of the variable. The peaks at higher spatial frequencies are an indication of the additional waveforms required to give the data its nonsinusoidal shape. In this case, only the lowest-frequency peak should be used to characterize the peak scale.

This rule applies to ecological data as well. For example, consider the predator density along a hypothetical intertidal transect. The maximum density is constant for 1 m, then abruptly shifts to a higher density for 1 m, then back to the original density for 1 m. This “square wave” pattern is repeated along the shore. Thus, this hypothetical shoreline has a predation scale of 1 m. The spatial autospectrum of this square wave would look qualitatively similar to that of Fig. A1B, C, with its

primary peak at 0.5 m^{-1} (although the density is constant for 1 m, the pattern of density repeats itself every 2 m).

We now return to the problem of aliasing. Consider the situation shown in Figure A2A. Two sine waves of different frequencies are sampled with a fixed spacing, Δx. In every case, the sampled points fall on *both* sine waves. In other words, given this sampling regime, we have no way of discerning whether our measured variation is associated with wave #1 (at a frequency below the Nyquist frequency) or wave #2 (at a frequency above the Nyquist frequency). Indeed, an infinite number of sine waves at still higher frequencies could yield the same measurements given the spacing Δx. Only if we were to sample at a smaller interval would we be able to discern exactly what frequency (or frequencies) contribute to the measured variation. This observation is the essence of the fact noted earlier: we cannot accurately discern the frequency of variation for fluctuations above the Nyquist frequency. Fig. A2 has further implications, however. If, in reality it is wave #2 that is present in our data (rather than wave #1), the variation due to this wave is still recorded in our measurements even though its frequency lies above the Nyquist frequency. In other words, just because fluctuations occur at a frequency above that which we can accurately discern, the variation associated with these frequencies still appears in our data. The variance associated with frequencies above the Nyquist frequency is *aliased* to frequencies below the Nyquist frequency.

The mechanism by which aliasing occurs is shown in Fig. A2B. A fluctuation at a frequency above f_g is sampled at a spacing Δx where Δx is not a precise multiple of the wavelength of the fluctuation. As a result, if the first sample falls at a peak of the fluctuation, the second sample will be taken slightly off peak, the third sample farther off peak, and so forth. The sampled points trace out a sinusoidal fluctuation at a low frequency, a frequency well below the Nyquist frequency.

This is the aliased signal. It can be shown (e.g., Bendat and Piersol 1986) that a frequency f below the Nyquist frequency can potentially be "contaminated" by fluctuations at $2f_g \pm f$, $4f_g \pm f$, $6f_g \pm f$, etc. Thus, if there is variance above the Nyquist frequency, the measured spectrum may deviate substantially from reality.

In practice, the problem of aliasing is controlled by filtering the measured data prior to analysis. For example, our measurements of species diversity, mussel density, mussel disturbance, and predation intensity are made using a quadrat 0.21 m x 0.30 m. In essence, the values obtained from these measurements are averages over this area, and variation at smaller scales is thereby filtered out. Similarly, in the wave-force measurements made in this study, the size of the apparatus is such that measured forces are averaged over a scale x_{min} of approximately 20 cm. Forces with a smaller spatial scale cannot affect the apparatus, and variation associated with them therefore cannot be aliased. Measurements of larval recruitment are made using settlement plates of finite dimension, x_{min}. Each measurement is thus an average value tied to this minimum scale, and higher frequency (= smaller scale) variations are filtered from the data. In all real-world measurements, the properties of the measuring apparatus place an upper limit, $f_{max} = 1/x_{min}$, on the frequency that can be measured, and it is thus only those frequencies between f_g and f_{max} that can be aliased. Although we cannot definitely rule aliasing out as a factor in our analyses, the shape of all of our spectra (in which the variance decreases rapidly with increased frequency within the range we have sampled), and the relatively narrow band of frequencies between f_g and f_{max} suggests that aliasing effects are negligible.

The brief description here of spectral analysis has been couched in terms of spatial variation. The technique can be equally well applied to variation through time. In this case, the abscissa of

Fig. 1 would measure time, t, and the scale of variation would be characterized by harmonics of the fundamental temporal frequency, f_f:

$$f_f = \frac{1}{t_{max}}. \qquad \text{(A8)}$$

The process is sampled at equally spaced intervals of time, Δt, and the total length of the time series is $(n\text{-}1)\Delta t = t_{max}$. In a temporal spectrum, a peak at a high frequency corresponds to a variable that fluctuates with only a short interval between occurrences, whereas a peak at low frequencies corresponds to a variable that fluctuates with a long interval between occurrences.

Nuts and Bolts

Each of our data series was divided into four segments (each with an even number of data points) with a 50% overlap among segments. A Hanning window was applied to each segment to avoid spectral artifacts due to any abrupt deviation of the data from the mean at the ends of the segments, and the spectral estimates were calculated for each segment and adjusted for the decrease in variance due to the Hanning window. See Bendat and Piersol (1986) or Priestley (1981) for a discussion of spectral windows. The overall spectral estimate at each harmonic is the average of the estimates for the four segments.

The choice of four segments was determined by the following factors. We desired to examine our data at as broad a range of scales as possible, and the maximal scale (the minimum spatial or temporal frequency) is set by the length of the data series. The fewer the number of segments we used, the longer each segment could be, and the larger the scale we could examine. However, there is a practical lower limit to the number of segments. The statistical confidence in each spectral estimate decreases as the number of segments decreases (Bendat and Piersol 1986, Priestley 1981). We found that the use of four segments yielded results that were consistent with

those using higher numbers of segments, whereas the use of three or fewer segments yielded results that were unacceptably noisy. Thus, for our data the use of four segments represents the optimal tradeoff between record length and statistical confidence. Common, alternative methods for increasing statistical confidence (band averaging or running averaging the spectrum from the full time series) result in the loss of high-frequency spectral estimates and (for the same statistical confidence) do not retain any additional information about low frequencies.

Note that the use of multiple segments affects the number of data points necessary to examine a process. If Δx is the time or distance between measurements, x_g (= $2\Delta x$) is the smallest time or distance at which frequency-specific information is available (the Nyquist scale, the grain), x_{max} is the largest scale for which information is desired (the extent), and the number of samples in a single segment encompassing all the data is $(2x_{max}/x_g)+1$. If, however, d segments are needed for the analysis ($d > 1$), and an overlap of 50% between segments is assumed (as used here), the total number of samples required is:

$$\text{total number of samples} = \frac{(d+1)x_{max}}{x_g} + 1. \qquad \text{(A9)}$$

Thus, when $d = 4$ (as we have used), approximately 2.5 times as many samples are required as one might naively assume to examine variation at a given maximum scale.

The confidence limits on each spectral estimate are determined by the number of degrees of freedom associated with that estimate. When estimates are based on the average of n segments (as they are here), there are $2n$ degrees of freedom (Bendat and Piersol 1986). The 95% confidence limits are (Bendat and Piersol 1986, p 286):

$$\frac{2n\hat{S}(f)}{\chi^2_{2n,0.025}} \le S(f) \le \frac{2n\hat{S}(f)}{\chi^2_{2n,0.975}} \qquad \text{(A10)}$$

Lastly, we note that spectral analysis provides the same information as the analysis of autocovariance, a form of analysis with which ecologists may be more familiar (see Appendix C). The Wiener-Kinchine relationships show that the autocovariance of a process is the inverse Fourier transform of the autospectrum (Bendat and Piersol 1986). Thus, for example, the measurements of spatial autocorrelation in intertidal snails made by Underwood and Chapman (1996) provide the same type of spatial information as the spectral measurements made in this study.

Literature Cited

Bendat, J. S. and A. G. Piersol. 1986. Random Data: Analysis and Measurement Procedures (2nd Edition). John Wiley and Sons, N. Y.

Press, W. H., S. A. Teukolsky, W. T. Vetterling, and B. P. Flannery. 1992. Numerical Recipes in Fortran. 2nd Edition. Cambridge University Press, Cambridge, UK.

Priestley, M. B. 1981. Spectral analysis and time series. Academic Press. New York, NY.

Underwood, A. J. and M. G. Chapman. 1996. Scales of spatial patterns of distribution of intertidal snails. Oecologia **107**:212-224.

Figure Legends

Figure A1. A. A periodic signal (a truncated sine wave) similar to the signal of solar irradiance. B. The spectrum of the signal shown in panel A. Note the existence of a dominant peak. The secondary peak at the first harmonic of the primary peak is a result of the nonsinusoidal shape of the signal. C. The spectrum of panel B plotted on log-log axes.

Figure A2. A. The measurements taken at the dots could be due either to the low-frequency wave 1, or the-high frequency wave 2. B. Sampling a high-frequency wave at too low a

frequency leads to an aliased signal. The variation due to the high-frequency wave (the solid line) appears to occur at a much lower frequency (the dashed line).

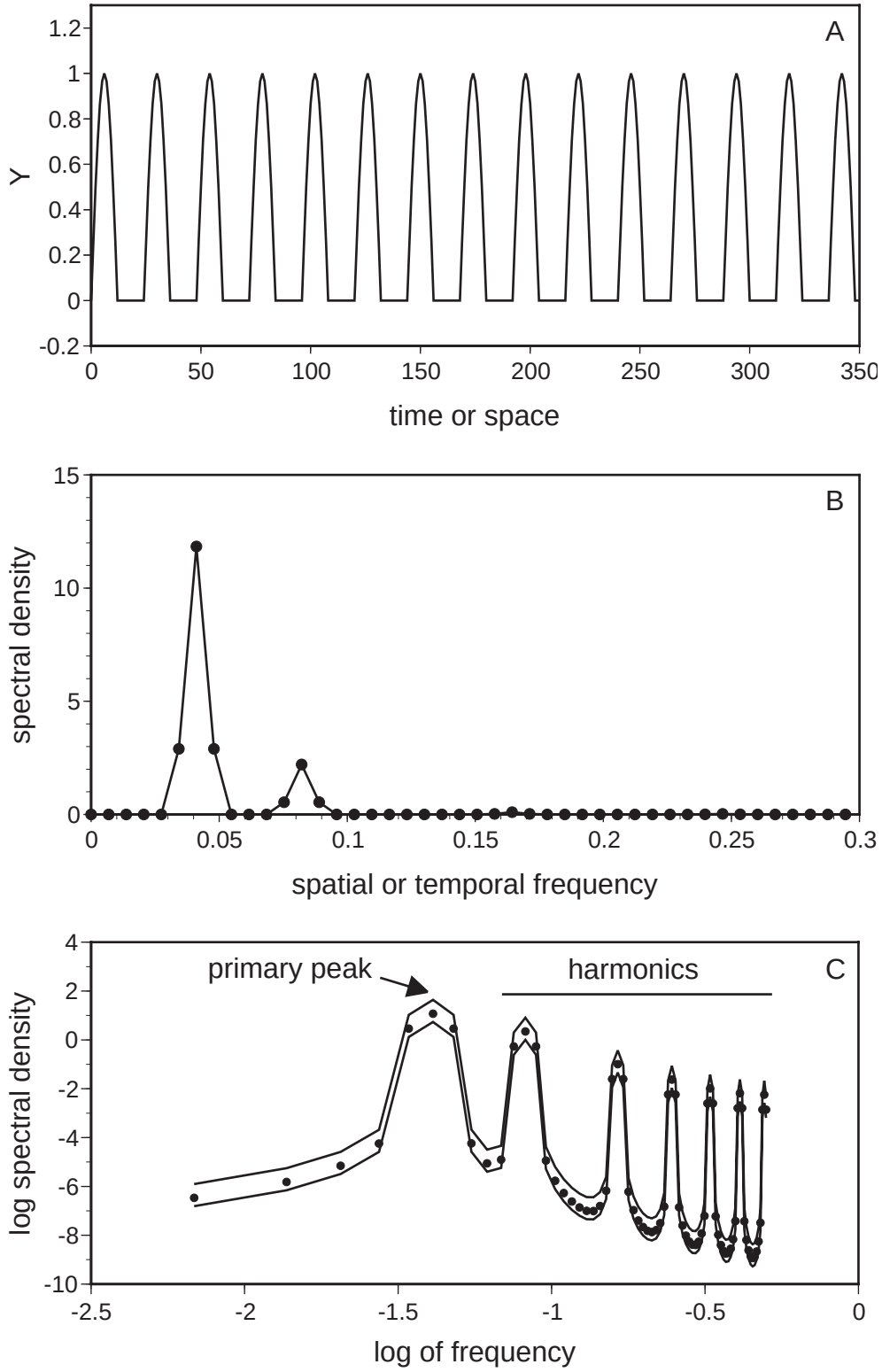
A
1.2
1
0.8
0.6
0.4
0.2
0
-0.2
Y
0
50
100
150
200
250
300
350
time or space
B
15
10
5
0
spectral density
0
0.05
0.1
0.15
0.2
0.25
0.3
spatial or temporal frequency
C
primary peak
harmonics
4
2
0
-2
-4
-6
-8
-10
log spectral density
-2.5
-2
-1.5
-1
-0.5
0
log of frequency

Fig. A1

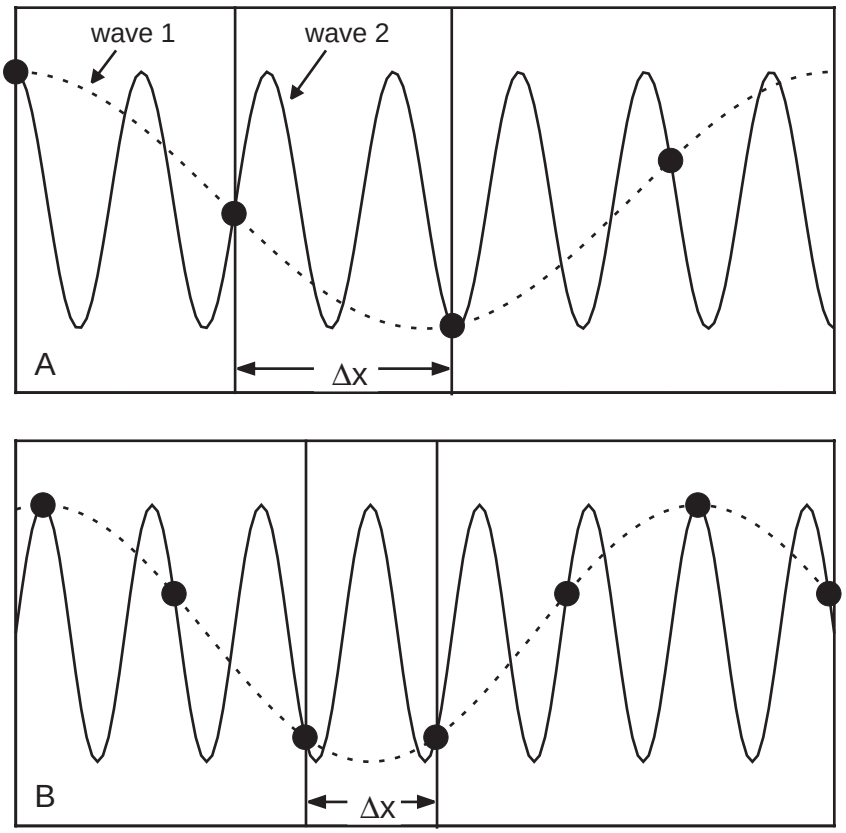

Fig. A2

Appendix B. Details of the Definitions of Scale

Practical implementation of the definitions of scale involves a number of details and caveats, which are discussed below.

1. The Peak Scale

Practical considerations and caveats regarding calculation of the spectrum itself have been covered in Appendix A. The fraction of the overall variance associated with each dominant spectral peak was calculated by integrating the area under the peak (the limits of which were judged by eye) and dividing that area by the integral of the entire spectrum.

Note that the definition of the peak scale requires that we be able to discern discrete peaks in the spectrum. When examining our spectra for the existence of discrete peaks, the following criteria were applied. If, on a log-log plot of the spectrum, the lower 95% confidence limit for a spectral estimate (see Appendix A) fell substantially above a regression line through the data, a peak was suspected, and if two adjacent spectral estimates met this criterion, the case for the existence of a peak was strengthened. In a few cases, the lower 95% confidence limit for a single estimate fell at or just marginally above the regression line, and in these cases we have taken a conservative approach and assume that these "peaks" are not sufficiently dominant to warrant the calculation of a peak scale. For each vetted peak we note the fraction of the overall variance contained within that peak. Only if a substantial fraction of the overall variance is contained within a peak (> approximately 25%), does the scale associated with that peak likely have much ecological significance.

2. The Frequency Scale

The frequency scale defined using Eq. 2 is affected by issues of practical measurement. The upper limit of integration is constrained by the highest frequency at which we can examine a

phenomenon. This limiting frequency (f_g, the Nyquist frequency, see Appendix A) corresponds to twice the smallest time or distance over which we make measurements. The Nyquist time or distance is in turn a measure of the grain of measurement. The lower limit of integration, f_{max}, is constrained by the largest time or distance over which we can measure a phenomenon (the extent). Given these practical limits, the average frequency of the measurable variation is

$$\overline{f} = \frac{\int_{f_{min}}^{f_g} fS(f)df}{\int_{f_{min}}^{f_g} S(f)df} \qquad \text{(B1)}$$

What are the effects of these limits of integration on the average frequency? The answer depends on the shape of the spectrum. If the spectral density is low in the vicinity of both the maximum and minimum frequencies, the presence of these constraints has negligible effect. In contrast, if the spectral density is substantial near either limit, the magnitude of the limit affects the calculated scale. For example, by inserting Eq. 8 into eqs. 2 and 3, we find that the frequency scale of a 1/*f*-noise process ($0 < \beta < 1$) is:

$$\overline{L}_f = \left[\frac{2-\beta}{2(1-\beta)}\right]\frac{f_g^{1-\beta} - f_{min}^{1-\beta}}{f_g^{2-\beta} - f_{min}^{2-\beta}} \qquad \text{(B2)}$$

An increase in either the grain (f_g) or the extent (f_{min}) of measurement results in an increase in the calculated frequency scale.

As f_{min} approaches 0 (that is, as the extent of the measurement gets very large), this expression reduces to:

$$\overline{L}_f = \frac{2-\beta}{2(1-\beta)} f_g^{-1} \qquad \text{(B3)}$$

In this case, the *f*-scale is independent of the extent of measurement, and the grain has the strongest influence on the calculated *f*-scale: the smaller the grain, the higher f_g is, and the smaller the scale. Note that when $\beta > 1$, the integral in the numerator of Eq. 2 is improper, and it cannot be used to calculate a scale for a measurement of infinite extent.

In light of these complications, the frequency scale of 1/*f*-noise processes must be treated with caution. In particular, one would expect that for any practical set of measurements the calculated scale will increase with an increase in either the grain or the extent of the measurements. The *f*-scale values subject to this cautionary note are indicated in Tables 1 and 2 with an asterisk.

3. The Wavelength Scale

As with the frequency scale, practical application of the definition of the wavelength scale (Eq. 4) is constrained by the grain and extent of measurement. The upper limit of integration is constrained by the extent, $\lambda_{\max}$, and the lower limit by the grain, λ_g:

$$L_w = \frac{\int_{\lambda_g}^{\lambda_{\max}} \lambda G(\lambda) d\lambda}{2 \int_{\lambda_g}^{\lambda_{\max}} G(\lambda) d\lambda} \tag{B4}$$

If the spectral density is substantial in the vicinity of these limits, the magnitude of the limits can affect the calculated scale. For example, if the spectrum is 1/*f* noise ($0 < \beta < 1$), L_w is

$$L_w = \left[\frac{\beta + 1}{2(\beta + 2)} \right] \frac{\lambda_{\max}^{\beta+2} - \lambda_g^{\beta+2}}{\lambda_{\max}^{\beta+1} - \lambda_g^{\beta+1}} \tag{B5}$$

An increase in either the extent or grain of measurement results in an increase in the calculated wavelength scale.

If the grain of the measurement is very small compared to the extent, this expression reduces to

$$L_w = \frac{\beta + 1}{2(\beta + 2)} \lambda_{\max} \qquad \text{(B6)}$$

Clearly, in this case the extent of the measurement is the strongest influence on the calculated wavelength scale.

4. The Integral Scale

The integral scale has been widely used in the study of turbulence as a measure of the characteristic scale of velocity fluctuations (Tennekes and Lumley 1972). In this application, it is generally assumed that the autocorrelation function asymptotically decays to 0 at infinite lag, and the parameter *a* in Eq. 5 is thus commonly cited as ∞. In contrast, ecological systems often exhibit autocorrelation functions that wander negative, leading us to the arbitrary selection of *a* used here.

As with the frequency-, and wavelength scales, the integral scale can be directly affected by the grain and extent of measurement. For the 1/*f*-noise spatial data typical of this study, the grain of measurement has little effect, whereas the calculated *i*-scale is sensitive to the measurement's extent: the larger the extent, the larger the *i*-scale. This effect is illustrated in Fig. B1. Here, the autocovariance for the 1/*f*-noise process has been estimated by numerically solving:

$$\gamma(\tau) = 2 \int_{f_{\min}}^{f_g} \left(\frac{\kappa}{f^{\beta}} \right) \cos(2\pi f \tau) df \qquad \text{(B7)}$$

This is the inverse Fourier transform of the spectrum, which, by the Wiener-Kinchine relationships is equal to the autocovariance (Bendat and Piersol 1986).

5. The Derivative Scale

The concept of the derivative scale is challenged by our ability to calculate the derivative for the type of discrete data that are available for ecological measurements. The standard finite-difference technique for estimating the derivative at a point is illustrated in Fig. B2. The value y_i of a process is measured at a series of points, x_i, where the spacing between measurements is a

constant Δx. For three adjacent points, the derivative at the middle point, x_i, is estimated as a three-point average:

$$\frac{dy}{dx} \cong \frac{(y_{i+1} - y_i) + (y_i - y_{i-1})}{(x_{i+1} - x_i) + (x_i - x_{i-1})} = \frac{(y_{i+1} - y_i) + (y_i - y_{i-1})}{2\Delta x} \qquad \text{(B8)}$$

This formula works well as long as the scale of variation is large relative to $2\Delta x$. However, when the measured quantity varies rapidly, Eq. B8 can lead to a gross underestimation of the average derivative of the process. No fully satisfactory solution is apparent for this problem. As a partial solution, we have chosen to calculate the derivative as a two-point average:

$$\frac{dy}{dx} \cong \frac{(y_{i+1} - y_i)}{\Delta x} \qquad \text{(B9)}$$

Use of this two-point derivative reduces the tendency to overestimate the derivative scale. The magnitude of the residual tendency is shown in Fig. B3. In plotting this figure, Eq. B9 has been used to calculate the derivative scale of a fixed wavelength monochromatic sine wave as the spacing between measurements is varied. The ratio of the sampled vs. the continuous scale is almost always greater than 1.0 (that is, the calculated derivative scale is too large), but the deviation from 1.0 is relatively small (on average, only 5%). This curve has been truncated at a measurement interval equal to half the wavelength, a spacing that places our measurements at the Nyquist frequency (see Appendix A).

6. The Variance Scale

In practice, the scheme described in the text is carried out through the use of spectral analysis. As described in Appendix A, the spectrum was calculated for a particular variable, and the standard deviation at a measurement scale *a* is defined as the square root of the sum of the variances at all smaller scales (higher frequencies):

$$\sigma(a) = \sqrt{\int_{1/a}^{\infty} S(f)df} \qquad \text{(B10)}$$

Characterization of the inflection point, a_i, in this curve was then carried out as described in the text. This procedure works well for our data, but there is no guarantee that it will work for all data.

The practical value of the inflection point in a curve of $\log\sigma$ vs. log measurement extent (e.g., Fig. 3) is as an estimate of the scale at which a phenomenon must be measured to ensure that most of the variation present in the real world is also present in one's data. This value is jeopardized if, as the extent of measurement increases beyond the variance scale, the variance continues to increase. Thus, the slope of the curve of $\log\sigma$ vs. log measurement extent at large extents can be used as an index of the "solidity" of our estimation of the *v*-scale. If this slope is small, the inflection point represents a solid estimate of the variance scale. If, in contrast, the slope is substantial, this is an indication that the standard deviation continues to increase with an increase in the extent of measurement, and our estimate of the *v*-scale is weak. In general, the slopes calculated for our temporal data are small, whereas the slopes for our spatial data are substantial (Table B1). The estimates of the spatial *v*-scale should therefore be taken with a grain of salt.

Comparisons Among Scales

When these definitions are applied to our data, the different methods often yield different estimates of scale. These differences are due to the nature of the data (in particular, the shape of the spectrum), and are not intrinsic to the definitions themselves. The sole exception to this statement is the derivative scale, which yields a value that is approximately 5% high, as noted above. This slight bias is negligible compared to the order-of-magnitude differences commonly found when these definitions are applied to real-world data. The precise manner in which a data series interacts with our definitions of scale is complex. However, we have conducted a preliminary exploration. First,

we calculated the scale for a simulated monochromatic, sinusoidal signal that varies with a 10-m wavelength, sampled as it would be on our transects. As expected, each definition of scale yields a reliable 5-m scale for each of the transect lengths for each of the *p*-, *f*-, *w*-, *v*-, and *i*-scale calculations.

We next applied our definitions to simulated 1/*f*-noise data following a method suggested by Hastings and Sugihara (1993). To construct each data series, we first created an appropriate Fourier series by choosing amplitude coefficients for a harmonic series of frequencies, f_i. The coefficient for each harmonic is the absolute value of a sample chosen from a normal distribution with a mean of zero and a variance equal to $1/f_i^{\beta}$. Each harmonic in the Fourier series was then assigned a random phase, uniformly distributed between 0 and 2π. The inverse Fourier transform of this series yielded one realization of a 1/*f*-noise data set with spectral exponent β. Thirty such data sets were created for each value of β for each method of calculating scale, and the average and standard deviation of calculated scales were determined. β values ranging from 0 to 2 were tested, and the results are given in Fig. 7. In all cases, the slope of log σ vs. log measurement extent was substantial for large values of *a*, suggesting that the estimates of the *v*-scale shown here are "weak," as discussed above.

Note that all of our definitions for the scale of variability can be related through the spectrum. This interrelationship is simply a mathematical acknowledgment of the fact that any definition of the scale of variability is tied to a description of pattern. A spectrum can be calculated for any natural pattern (periodic or otherwise) (Priestley 1981, Bendat and Piersol 1986), thus the existence of a spectrum does not imply that a pattern is periodic.

Literature Cited

Bendat, J. S. and A. G. Piersol. 1986. Random Data: Analysis and Measurement Procedures (2nd Edition). John Wiley and Sons, N. Y.

Hastings, H. M. and G. Sugihara. 1993. Fractals: a user's guide for the natural sciences. Oxford University Press, Oxford.

Priestley, M. B. 1981. Spectral analysis and time series. Academic Press. New York, NY.

Tennekes, H. and J. L. Lumley. 1972. A first course in turbulence. MIT Press, Cambridge, MA.

Table B1. Parameters related to the "solidity" of the *v*-scale estimate. The lower the ratio of slopes, the better the estimate. High slopes > 0 indicate that variability continues to increase with measurement scale, and the calculated *v*-scale thus incorporates only a fraction of the total variability.

	High Slope	Low Slope	Ratio
Solar Irradiance	0.012	102.00	0.000117
Intertidal Body Temp	0.045	204.00	0.000220
Upwelling Index	0.050	7.16	0.006980
Sea Surface Temp.	0.018	317.00	0.000057
Significant Wave Height	0.007	251.00	0.000028
Force			
short	0.405	8.44	0.048000
medium	0.189	5.55	0.034100
long	0.300	4.10	0.073000
Wave Force Index			
short	0.176	3.46	0.050800
medium	0.201	3.45	0.058300
long	0.195	6.06	0.032200
Temperature			
short	0.446	6.47	0.068900
medium	0.274	5.81	0.047200
Chlorophyll			
medium	0.488	6.11	0.079900
Diversity			
short	0.108	6.71	0.016000
medium	0.087	5.30	0.016400
long	0.165	7.33	0.022900
Mussel Density			
short	0.128	3.45	0.037100
medium	0.244	6.75	0.036100
long	0.258	7.22	0.026600

Table B1 continued.

Mussel Disturbance			
short	0.074	1.82	0.040700
medium	0.078	4.83	0.016100
long	0.140	8.05	0.017400
Mussel Recruitment			
medium	0.159	2.95	0.053900
Predators			
short	0.095	5.47	0.017400
medium	0.695	6.32	0.011000
long	0.035	2.38	0.014700
Grazers			
short	0.052	4.52	0.011500
medium	0.298	11.30	0.026200
long	0.112	3.84	0.029200

Figure Legends

Figure B1. The integral scale is affected by the extent of measurement for 1/*f*-noise processes. To produce these curves 1/*f*-noise signals with a maximum extent of 5000 m were sampled at a range of measurement extents.

Figure B2. A schematic representation of the factors used to calculate a derivative for discretely sampled data (see text).

Figure B3. Estimation of the derivative using finite difference leads to an overestimate of the derivative scale. The ratio of the sampled, calculated scale to the actual scale is shown as a function of the relative magnitude of the measurement interval to the wavelength of the sinusoidal signal.

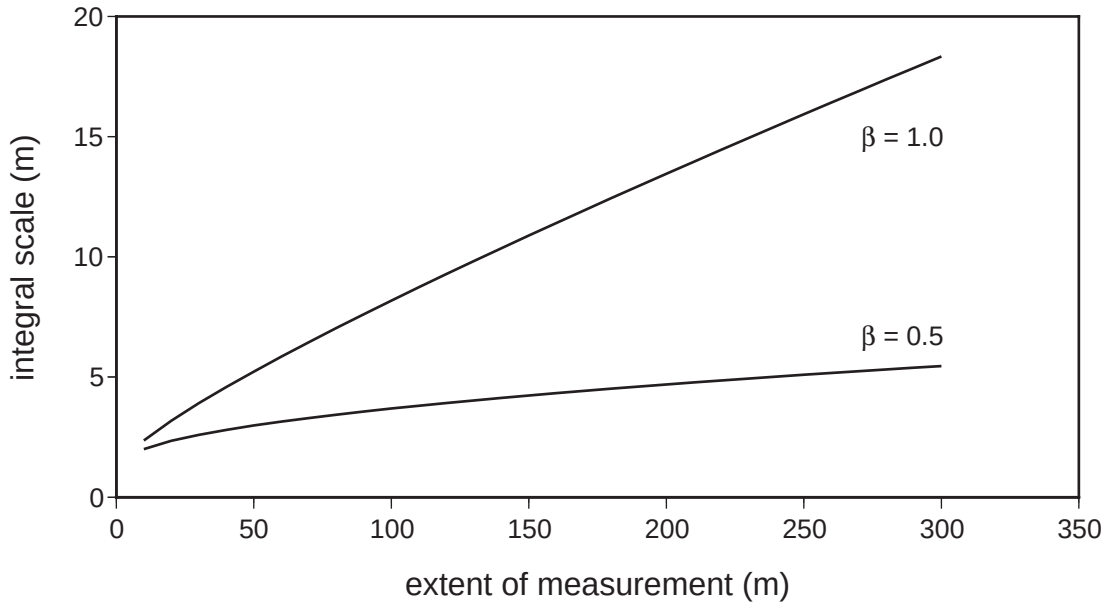
20
15
10
5
0
integral scale (m)
β = 1.0
β = 0.5
0
50
100
150
200
250
300
350
extent of measurement (m)

Fig. B1

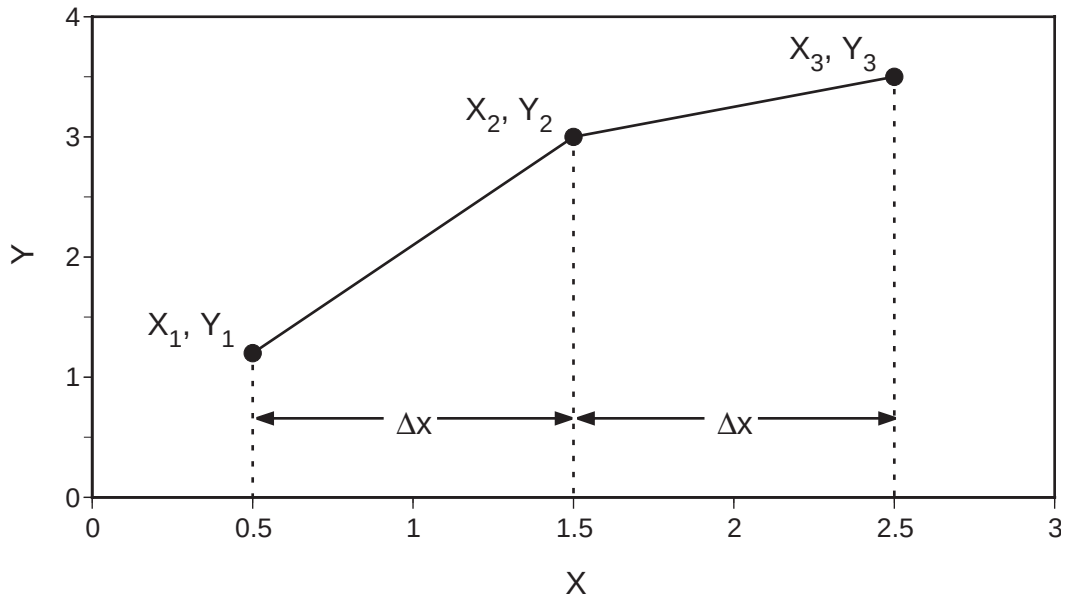

Fig. B2

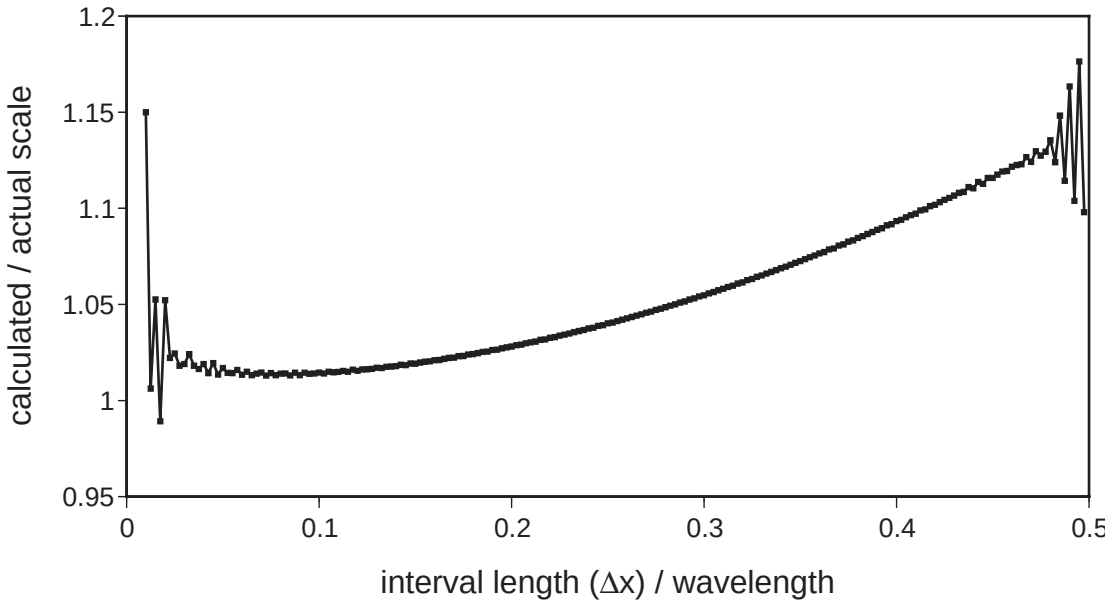
1.2
1.15
1.1
1.05
1
0.95
calculated / actual scale
0
0.1
0.2
0.3
0.4
0.5
interval length (Δx) / wavelength

Fig. B3

Appendix C. Autocorrelation

The autocorrelation function is a measure of how well points in a series of data are correlated to other points in the same series, separated by a certain lag. Consider a set of n measurements, $x_1, x_2, \ldots x_n$, taken at equal intervals in either time or space. The autocovariance for a lag, r, is

$$\gamma(r) = \frac{1}{n-r}\sum_{i=1}^{n-r}(x_i - \mu_x)(x_{i+r} - \mu_x) \qquad \text{(C1)}$$

where μ_x is the mean of the data series.

The autocovariance can be expressed as a fraction of the overall variance to give the autocorrelation:

$$\rho(r) = \frac{\gamma(r)}{\sigma^2} = \frac{\gamma(r)}{\frac{1}{n}\sum_{i=1}^{n}(x_i - \mu_x)^2} \qquad \text{(C2)}$$

Appendix D: Details of the Materials and Methods

1. Recording Dynamometers.

At each experimental location on the transects, a 1.6-cm diameter, 20-cm deep hole was drilled into the granite substratum. The opening of this hole was countersunk to a depth of 2.5 cm and a diameter of 3.2 cm, and a PVC threaded female pipe fitting (1/2" NPT) was installed using epoxy putty. This fitting served to mount either a recording dynamometer (for measurements of maximum wave-induced hydrodynamic force), or a recording thermometer (for measurements of maximum temperature).

The recording dynamometers were similar in construction to those described by Bell and Denny (1994) and Denny and Wethey (2000). A drag element (a wiffle golf ball) was connected by a short length of fishing line to a spring housed in a short length of plastic pipe. Any force imposed on the ball stretched the spring, and the maximum was recorded by a rubber slider on the fishing line. The housing fit snugly into a hole in the substratum. Details of the construction of the device can be found in Bell and Denny (1994) or at www.stanford.edu/group/Denny.

To make a measurement, the slider was reset using forceps and the device was screwed into its emplacement. After an appropriate period (typically 4 - 10 days), the device was recovered and the position of the slider was measured using Vernier calipers. The larger the force imposed on the drag element, the larger the displacement of the slider. The proportionality between applied force and displacement was determined in the laboratory for each device by holding the device ball-down and hanging known weights from the ball. There are two salient differences between the device described by Bell and Denny and that used here. First, the housing of the current device is mounted rigidly in the substratum. Because the whole device does not need to reorient with the flow during the passage of a wave, the response time of the current model is substantially less than that of the Bell/Denny device. Second, the shorter length of fishing line used in the current device (in the absence of drag, the ball is held less than 1 cm from the housing), allows the device to be installed in close proximity to organisms on the substratum. The "sweep" of the drag element when subjected to a large force is approximately 10 cm, suggesting that the spatial extent of the measurements made by an individual dynamometer is a circle with a diameter of approximately 20 cm.

2. Wave Gauge.

The calculation of significant wave height involves a correction for the attenuation of the wave-induced pressure signal as a function of depth. To avoid the possibility of artifacts due to this correction, the calculation of significant wave height was truncated at a wave frequency equal to approximately three times the peak frequency of the waves.

3. Recording Thermometers.

The thermometers were housed in 1.3-cm diameter CPVC pipes of the same length used for the dynamometers, and were similarly held in place by threaded male pipe fittings. The bulb of the thermometer extended out of the housing into a hole drilled into a 2.5-cm diameter brass ball. The ball (which was rigidly attached to the male pipe fitting by a threaded brass coupling) served both to protect the bulb of the thermometer and to ensure that the area of the device exposed to solar irradiance was independent of the angle at which the device was installed in the substratum. The brass ball was coated with a thin layer of matte-black rubber. To make a recording, the thermometer was briskly shaken to reset the column of mercury, and the housing was screwed into the emplacement in the substratum. The device was retrieved at a later time (typically 1 - 7 days), and the maximum temperature was recorded.

4. Topography.

The topography of the substratum was measured along all transects. The objective of these measurements was to create an index of the topographic potential for a given location to be exposed to wave-induced hydrodynamic forces. Experience led us to believe that this index should include (1) the horizontal angle (azimuth) of the local shore relative to the direction of wave approach, (2) the slope of the substratum at the location, and (3) the presence or absence of offshore obstacles in the path of wave approach. A location with a vertical slope facing directly into oncoming waves with no offshore obstacles has the greatest potential to encounter large forces, whereas locations

with lesser slopes facing obliquely to the waves and sheltered by obstructions have less potential. We propose that the following topographic index appropriately quantifies these ideas:

$$W = \frac{[\cos(\theta_w - \theta_s) \times \sin \phi_s] - c \sin \phi_b + 1 + c}{2 + 2c}. \qquad \text{(D1)}$$

Here θ_w is the compass direction from which waves approach the shore, θ_s is the compass angle of the horizontal component of the location normal, and ϕ_s is the slope of the shore at the location ($0 \le \phi_s \le 90^o$). ϕ_b is the blocking angle, the slope of a line drawn from the location to the top of the nearest "up-wave" obstacle ($-90 \le \phi_b \le 90^o$). If the location is on a vertical surface facing into the oncoming waves, this line would be drawn directly down from the site to the water below ($\phi_b = -90^\circ$). If the location is on a vertical surface facing away from the waves, the line is drawn vertically up ($\phi_b = 90^\circ$). W varies between 0 and 1. As proposed, the index is highest for vertical locations ($\phi_s = 90^o$) that face the oncoming waves ($\theta_w = \theta_s$) without obstacles ($\phi_b = -90^o$) and is lowest for vertical locations on the down-wave sides of obstacles. The value of c (which weights the contribution of offshore obstacles to the index) was chosen to provide the greatest correlation between W and maximum wave force. A value of $c = 0.6$ was used here. See Helmuth and Denny (2003) for details of this index and its measurement.

5. Microalgal Primary Productivity .

Microalgal primary productivity was estimated as the rate of algal film accumulation in the absence of herbivores. A 7.5 cm square settlement plate was installed at each location to measure the monthly accumulation of algal film. Each plate was made of 0.5 cm thick polycarbonate plastic (Lexan) covered with gray, rugose, safety-walk sheet (3M Corp.). These plates are a standard apparatus for measuring the recruitment of barnacles (Roughgarden et al. 1988). Each settlement plate was attached to the rock by a stainless steel threaded rod, which had been glued into a hole

drilled into the substratum. A 10 cm square sheet of copper foil was sandwiched between the settlement plate and the substratum. The resulting 1.25 cm border of copper served as an effective barrier to molluscan grazers.

Upon retrieval, the microalgal film was removed by scrubbing the plates with a small brush and the algal tissue, mixed with seawater, was concentrated by spinning at 2500 rpm in a refrigerated centrifuge. After pouring off the supernatant, the algal tissue was extracted in spectrophotometric grade acetone (90%). To ensure complete extraction, the volume of acetone ranged from 5 – 50 ml, depending on the volume of the algal sample. Extractions were done at –20 ^{o}C in complete darkness for 24 hours. The concentration of chlorophyll *a* in the absence of grazing, assumed to be a rough proxy for microalgal primary productivity, was determined spectrophotometrically using standard techniques (Hill and Hawkins 1990).

6. Temporal Variation in Physical Processes

Temperatures representative of the body temperature of intertidal organisms were measured in February, 2002. A brass ball (2.5 cm diameter) was painted flat black and tapped with a ½" NPT pipe thread. A small temperature logger (iButton, Dallas Semiconductor) was inserted in this hole and the ball was then mounted (using a threaded PVC coupling) on the intertidal rock at one of the locations on our transects. This "body" temperature was recorded to the nearest 0.5^{o}C every 10 minutes for two weeks in February 2002.

Gaps in the wave record from the Farallon Islands (due to equipment failure) were filled by linear interpolation. 11.7% of the time series was affected by gaps. The largest single gap was 3.3% of the overall time series.

Literature Cited

Bell, E. C. and M. W. Denny 1994. Quantifying "wave exposure": a simple device for recording maximum velocity and results of its use at several field sites. Journal of Experimental Marine Biology and Ecology **181**:9-29.

Denny, M. and D. Wethey. 2000. Physical processes that generate patterns in marine communities. pp. 3-37 in M. Bertness, S, Gaines, and M. Hay (eds.) Marine Community Ecology. Sinauer Asssociates, Sunderland, MA.

Helmuth, B. and M. W. Denny. 2003. Predicting wave exposure in the rocky intertidal zone: do bigger waves always lead to larger forces? Limnology and Oceanography (in press).

Hill, A. S. and S. J. Hawkins. 1990. An investigation of methods for sampling microbial films on rocky shores. Journal of the Marine Biological Association of the United Kingdom **70**:77-88.

Roughgarden, J., S. Gaines, and H. Possingham. 1988. Recruitment dynamics in complex life cycles. Science **241**:1460-1466.

Appendix E. Data Series and Spectra

The data series and associated spectra for our variables are shown in Figs. E1-E15.

Figure Legends

Figure E1. The signal, temporal spectrum, and log-log spectrum for solar irradiance at Hopkins Marine Station.

Figure E2. The signal, temporal spectrum, and log-log spectrum for intertidal "body" temperature at Hopkins Marine Station.

Figure E3. The signal, temporal spectrum, and log-log spectrum for sea-surface temperature at Hopkins Marine Station.

Figure E4. The signal, temporal spectrum, and log-log spectrum for significant wave height at the Farallon Islands.

Figure E5. The signal, temporal spectrum, and log-log spectrum for monthly measurement of the upwelling index.

Figure E6. The signal, spatial spectrum, and log-log spectrum for maximum wave forces on the three transects at Hopkins Marine Station.

Figure E7. The signal, spatial spectrum, and log-log spectrum for the topographic index on the three transects at Hopkins Marine Station.

Figure E8. The signal, spatial spectrum, and log-log spectrum for relative maximum temperature on two of the transects at Hopkins Marine Station.

Figure E9. The signal, spatial spectrum, and log-log spectrum for microalgal productivity on the medium transect at Hopkins Marine Station.

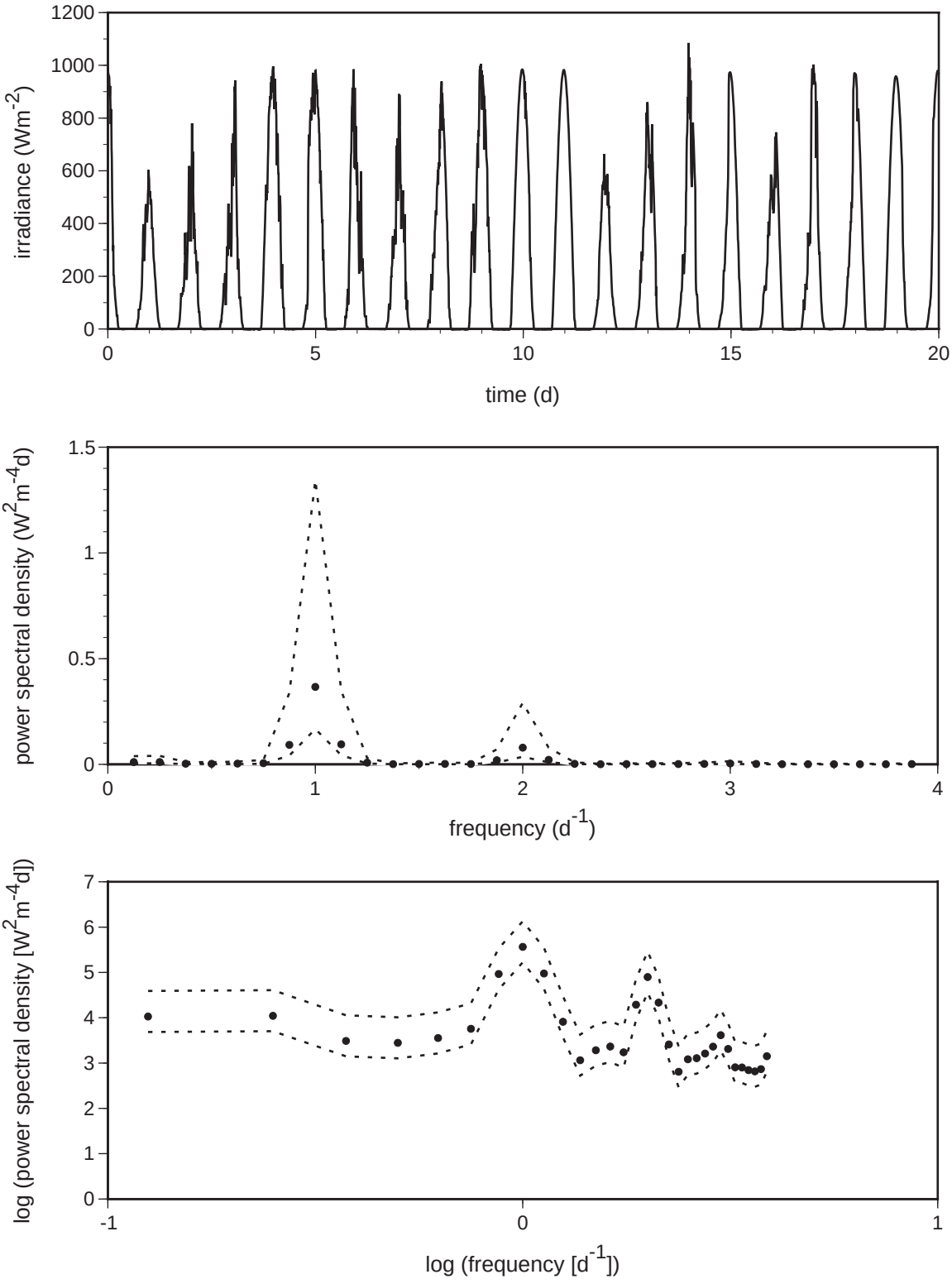
irradiance (Wm-2)
1200
1000
800
600
400
200
0
0
5
10
15
20
time (d)
power spectral density (W2m-4d)
1.5
1
0.5
0
0
1
2
3
4
frequency (d-1)
log (power spectral density [W2m-4d])
7
6
5
4
3
2
1
0
-1
0
1
log (frequency [d-1])

Fig. E1

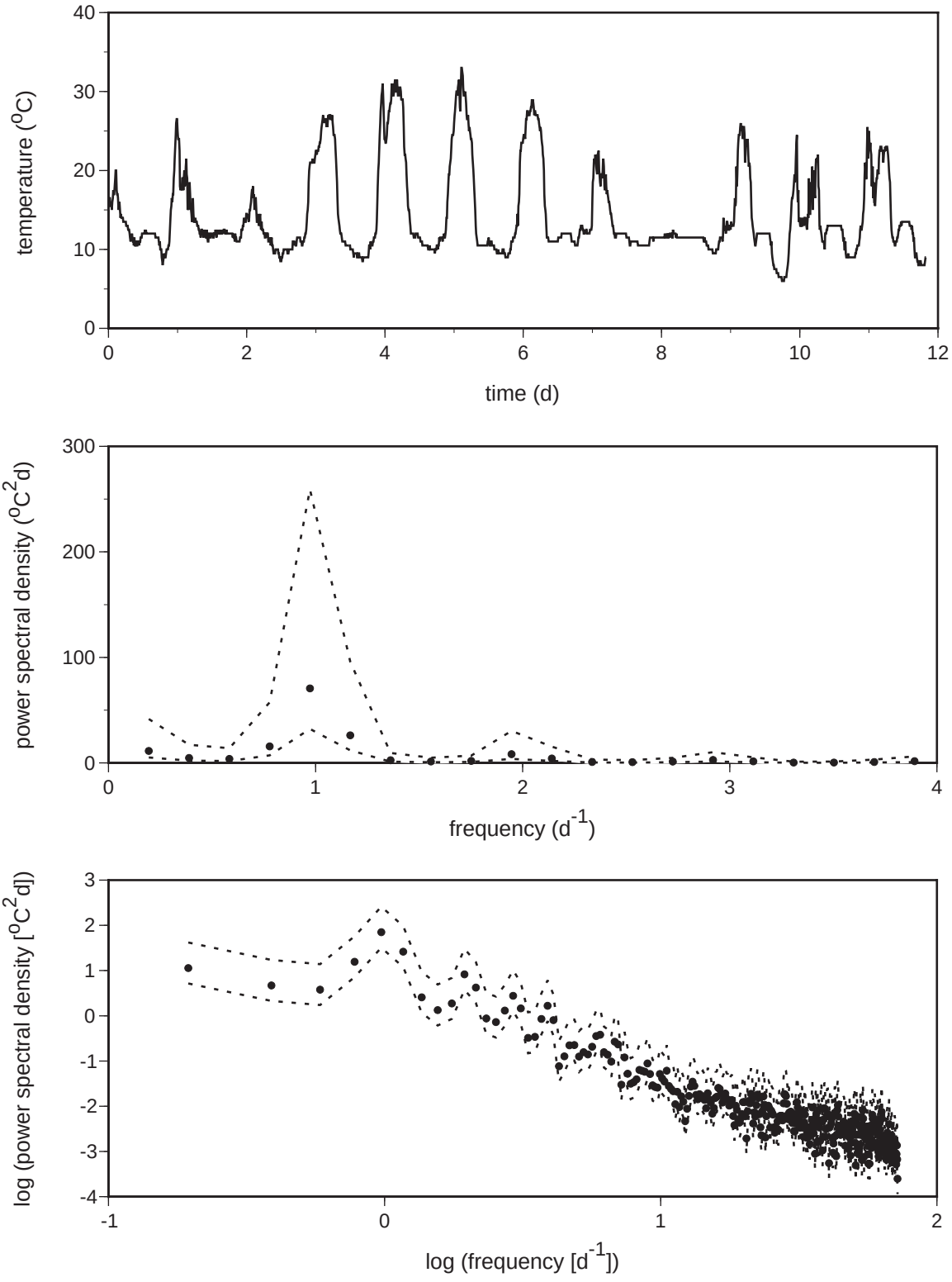
temperature (°C)
time (d)
power spectral density (°C² d)
frequency (d⁻¹)
log (power spectral density [°C² d])
log (frequency [d⁻¹])

Fig. E2

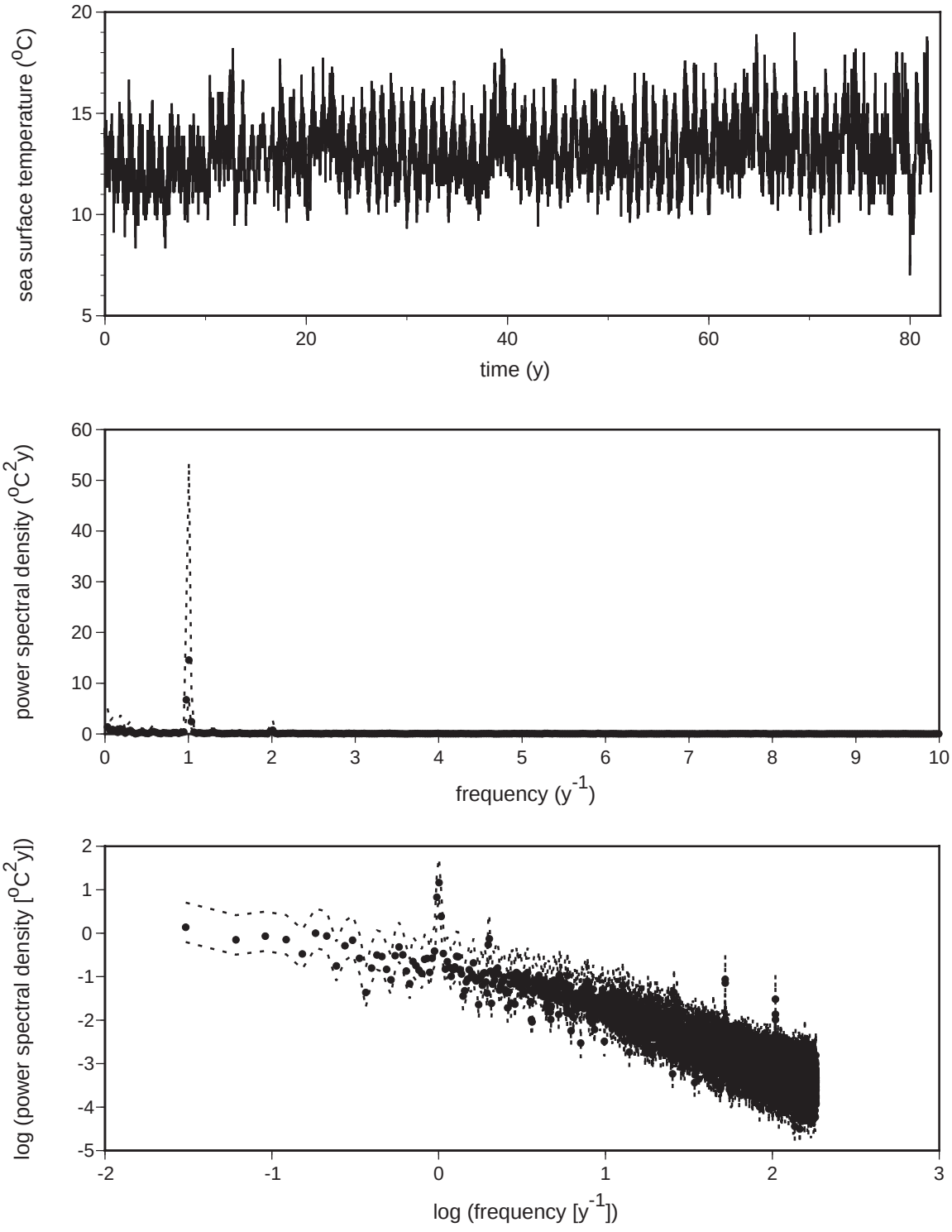
sea surface temperature (°C)
20
15
10
5
0
20
40
60
80
time (y)
power spectral density (°C²y)
60
50
40
30
20
10
0
0
1
2
3
4
5
6
7
8
9
10
frequency (y⁻¹)
log (power spectral density [°C²y])
2
1
0
-1
-2
-3
-4
-5
-2
-1
0
1
2
3
log (frequency [y⁻¹])

Fig. E3

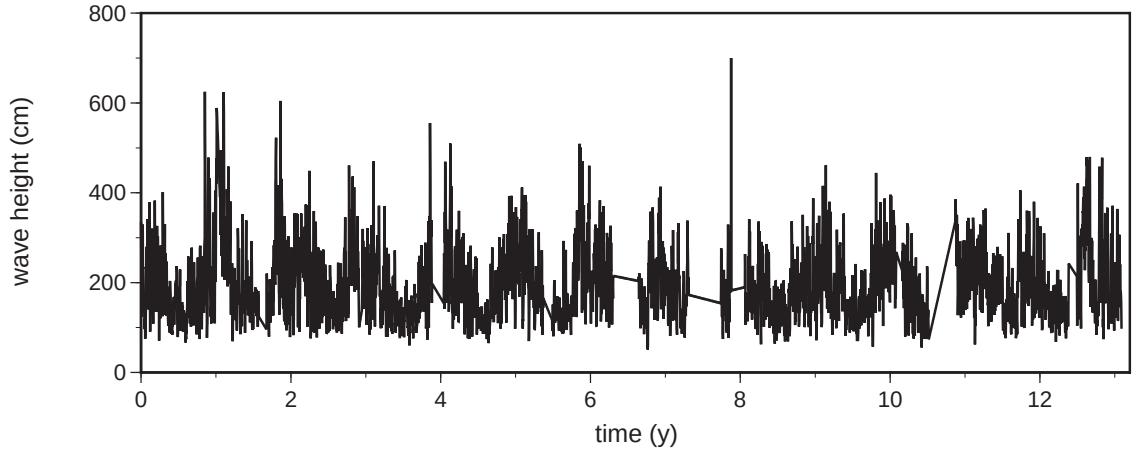
wave height (cm)
800
600
400
200
0
0
2
4
6
8
10
12
time (y)

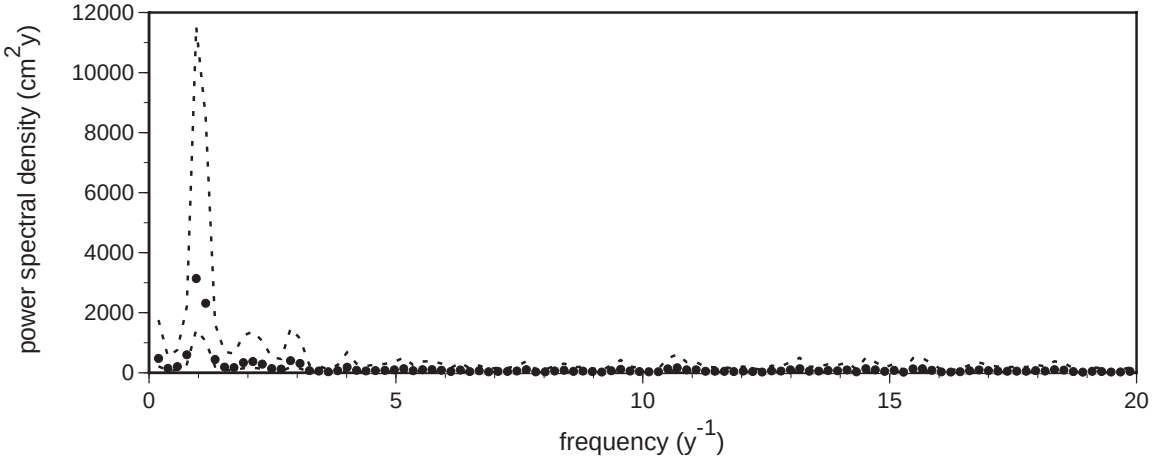
power spectral density (cm2y)
12000
10000
8000
6000
4000
2000
0
0
5
10
15
20
frequency (y-1)

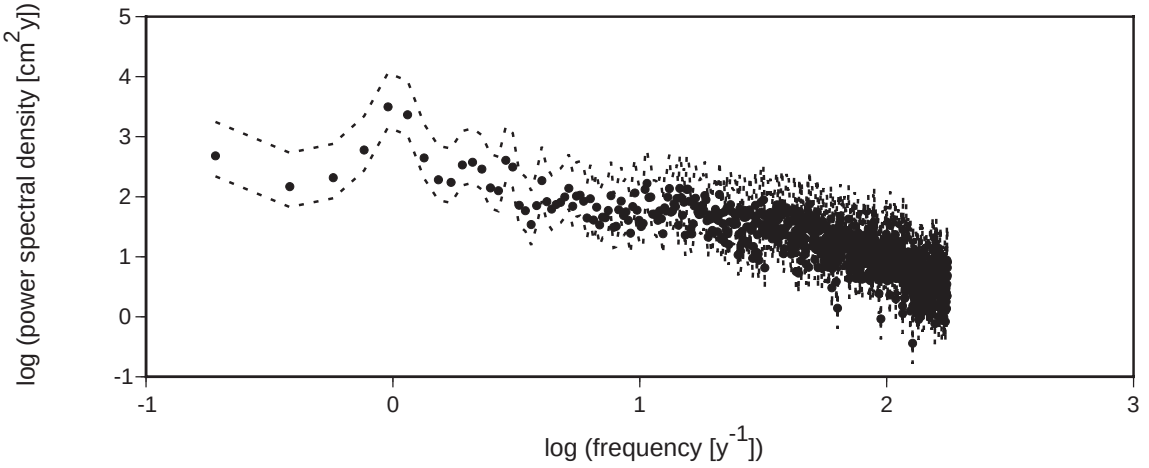
log (power spectral density [cm2y])
5
4
3
2
1
0
-1
-1
0
1
2
3
log (frequency [y-1])

Fig. E4

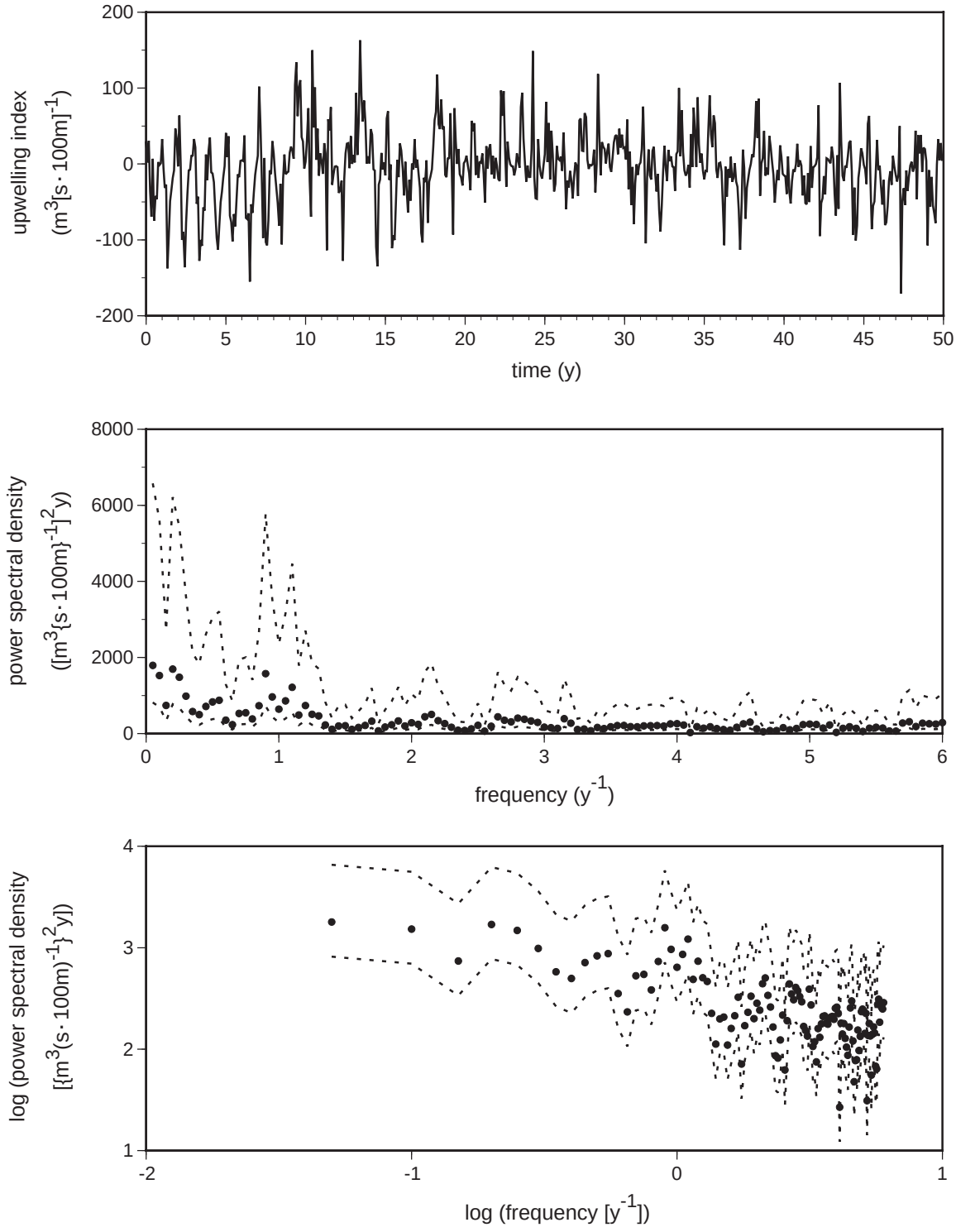
upwelling index
(m3[s·100m]-1)
200
100
0
-100
-200
0
5
10
15
20
25
30
35
40
45
50
time (y)
power spectral density
([m3{s·100m}-1]2y)
8000
6000
4000
2000
0
0
1
2
3
4
5
6
frequency (y-1)
log (power spectral density
[{m3(s·100m)-1}2y])
4
3
2
1
-2
-1
0
1
log (frequency [y-1])

Fig. E5

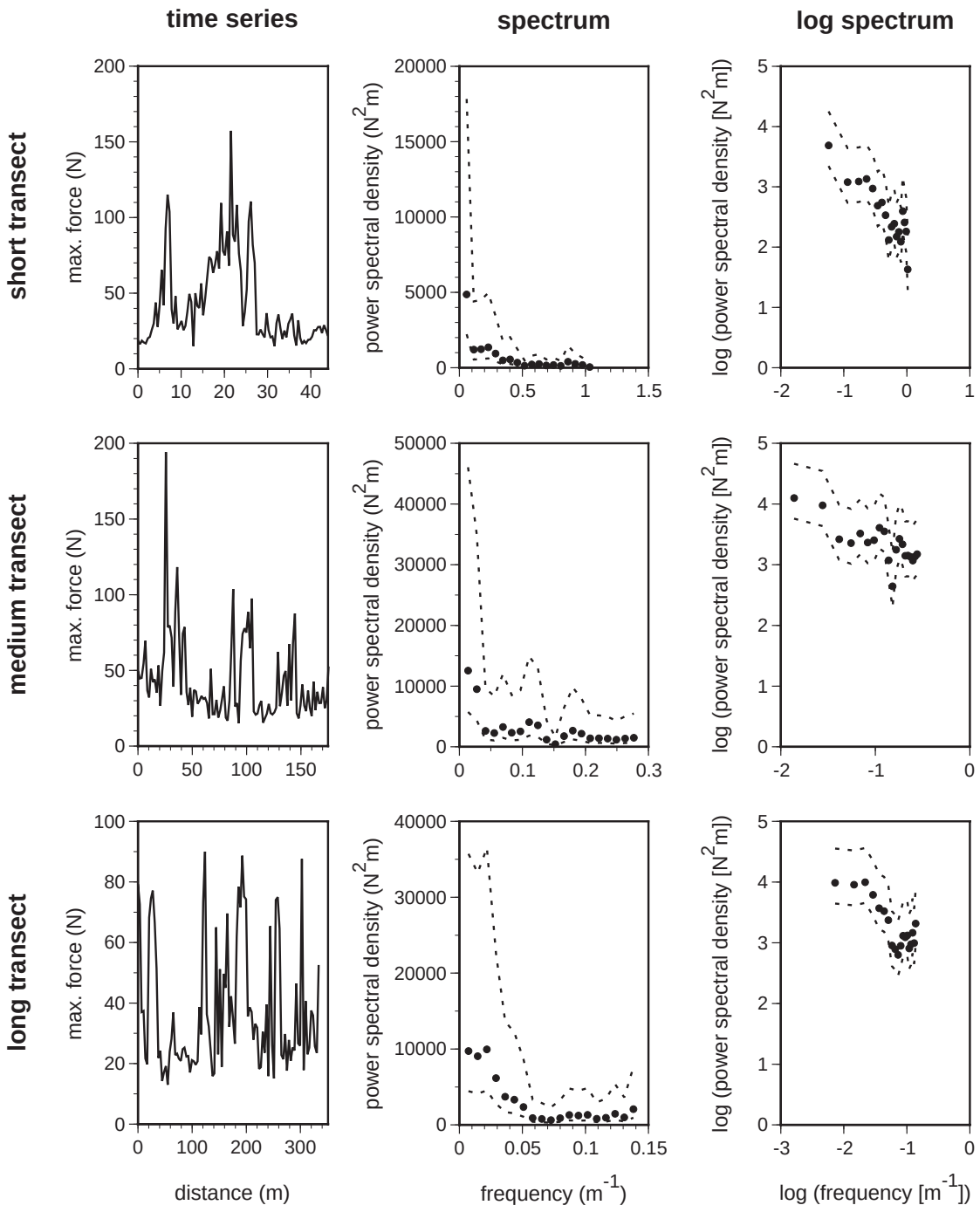
time series
spectrum
log spectrum
short transect
medium transect
long transect
max. force (N)
power spectral density (N²m)
log (power spectral density [N²m])
distance (m)
frequency (m⁻¹)
log (frequency [m⁻¹])

Fig. E6

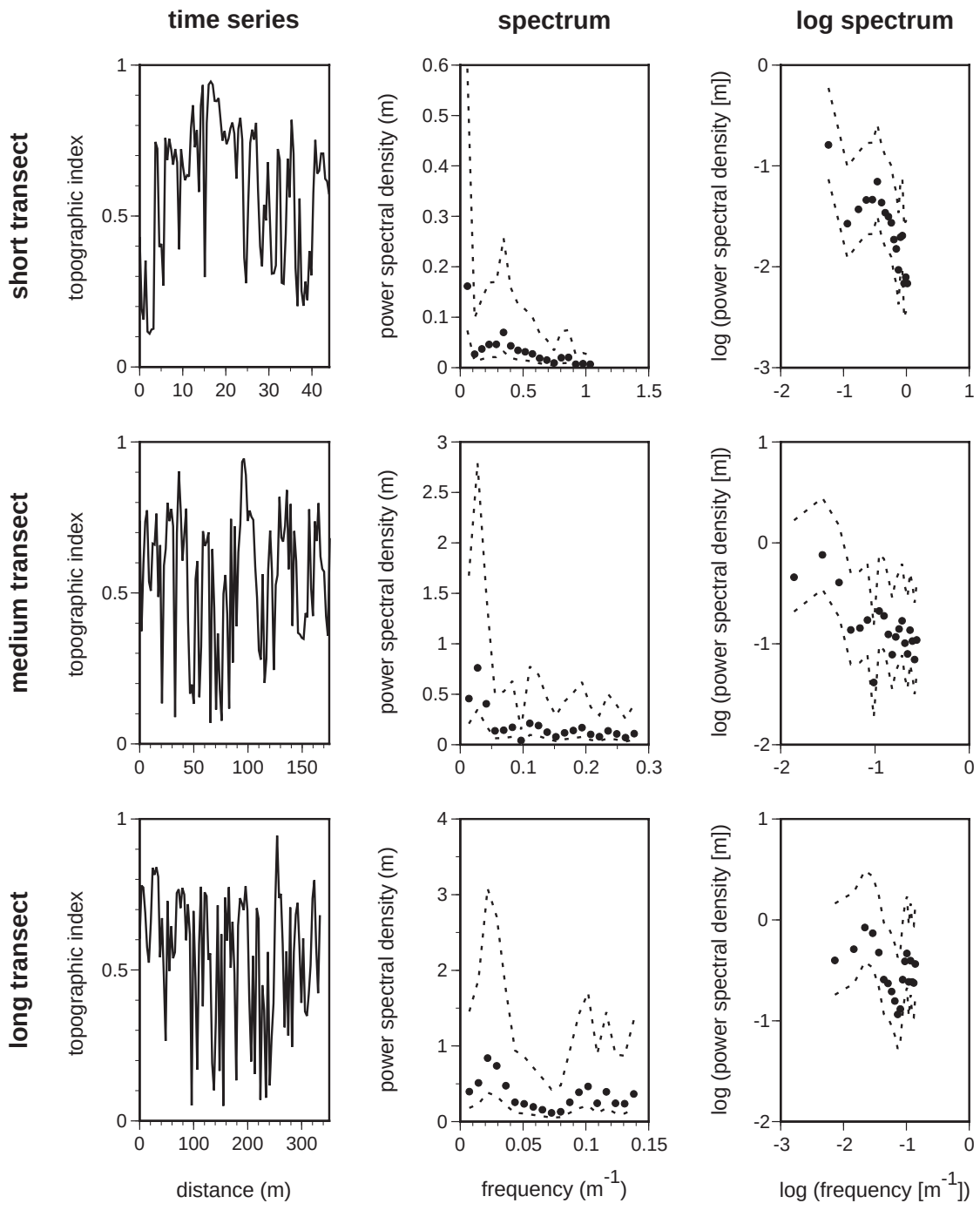
time series
spectrum
log spectrum
short transect
medium transect
long transect
topographic index
power spectral density (m)
log (power spectral density [m])
distance (m)
frequency (m-1)
log (frequency [m-1])

Fig. E7

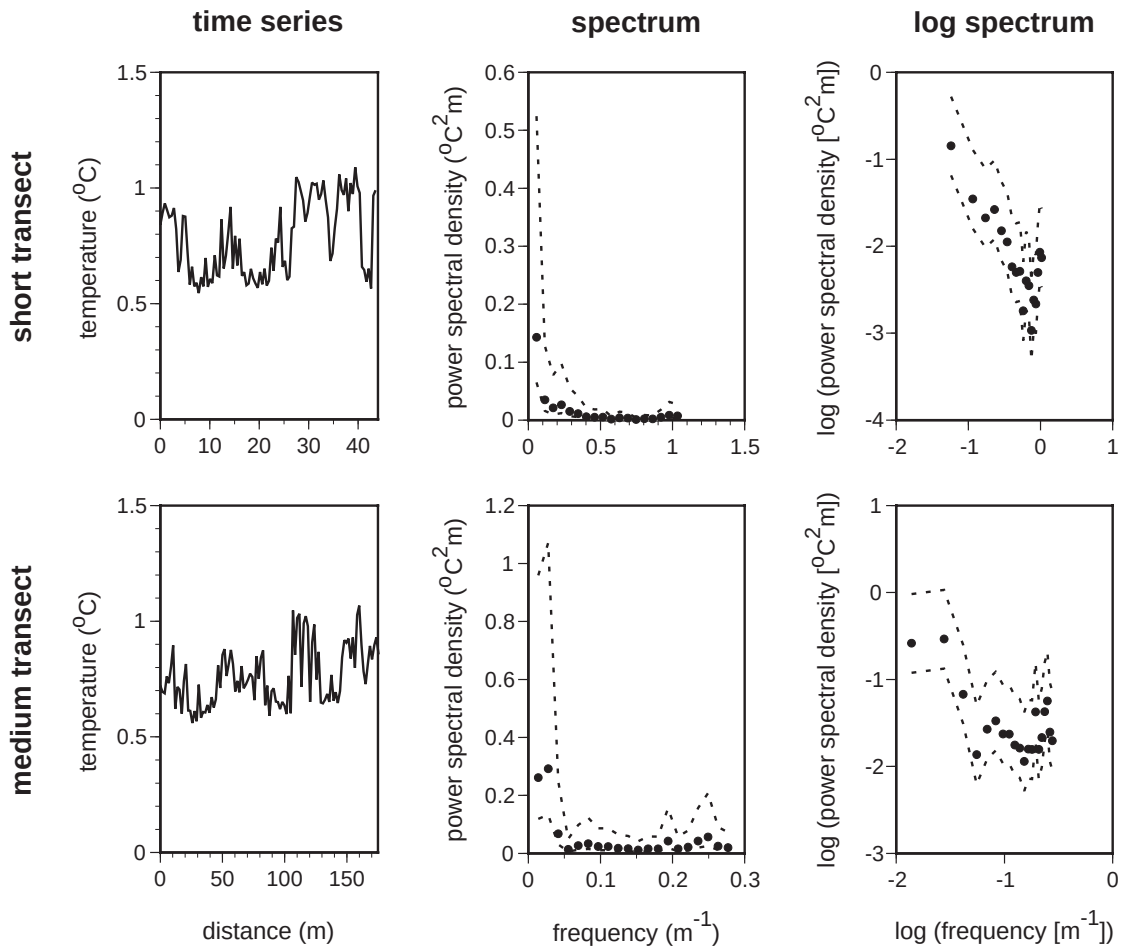
time series
spectrum
log spectrum
short transect
medium transect
temperature (°C)
power spectral density (°C²m)
log (power spectral density [°C²m])
distance (m)
frequency (m⁻¹)
log (frequency [m⁻¹])

Fig. E8

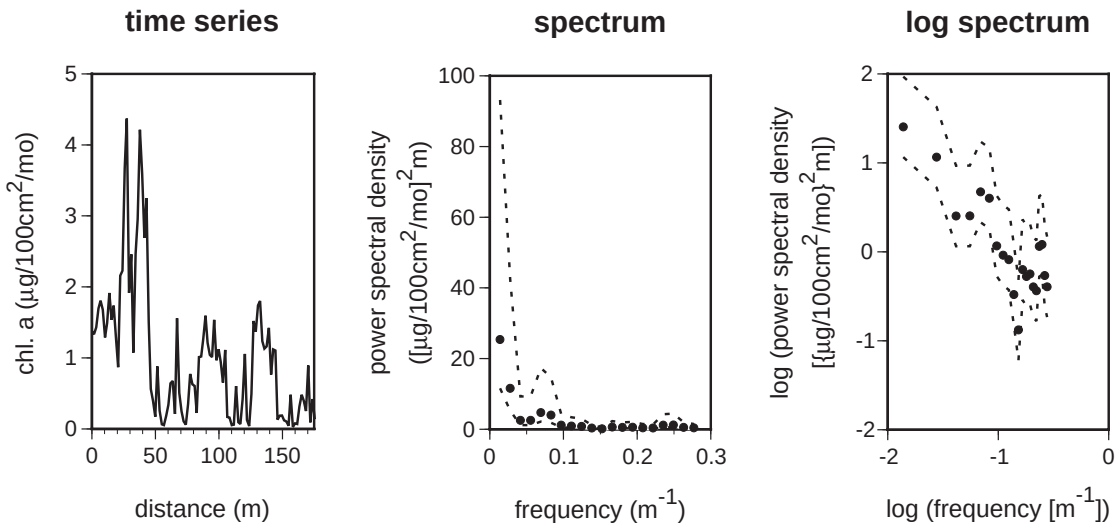
time series
spectrum
log spectrum
chl. a (µg/100cm2/mo)
distance (m)
power spectral density ([µg/100cm2/mo]2m)
frequency (m-1)
log (power spectral density [{µg/100cm2/mo}2m])
log (frequency [m-1])

Fig. E9

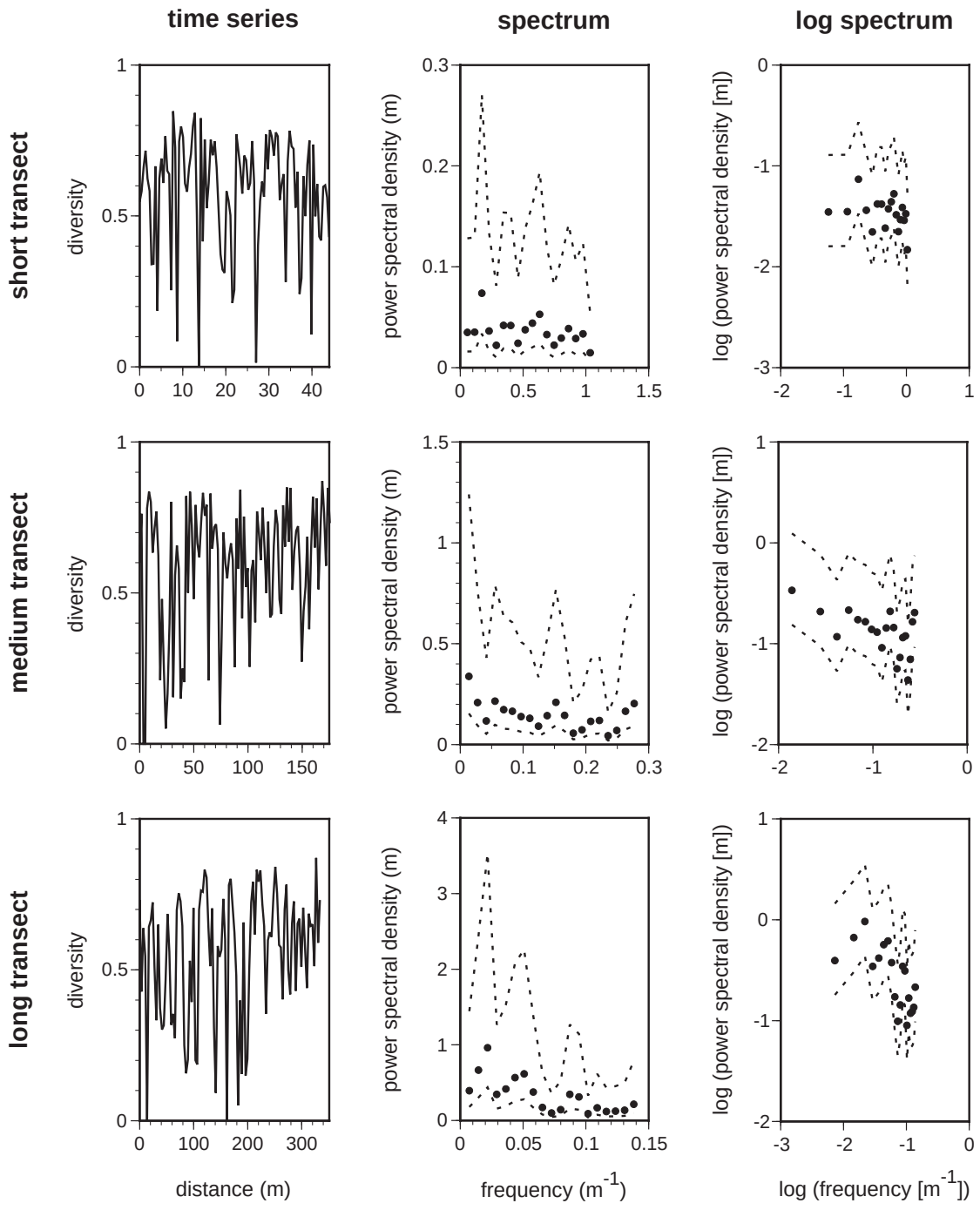
time series
spectrum
log spectrum
short transect
medium transect
long transect
diversity
power spectral density (m)
log (power spectral density [m])
distance (m)
frequency (m-1)
log (frequency [m-1])

Fig. E10

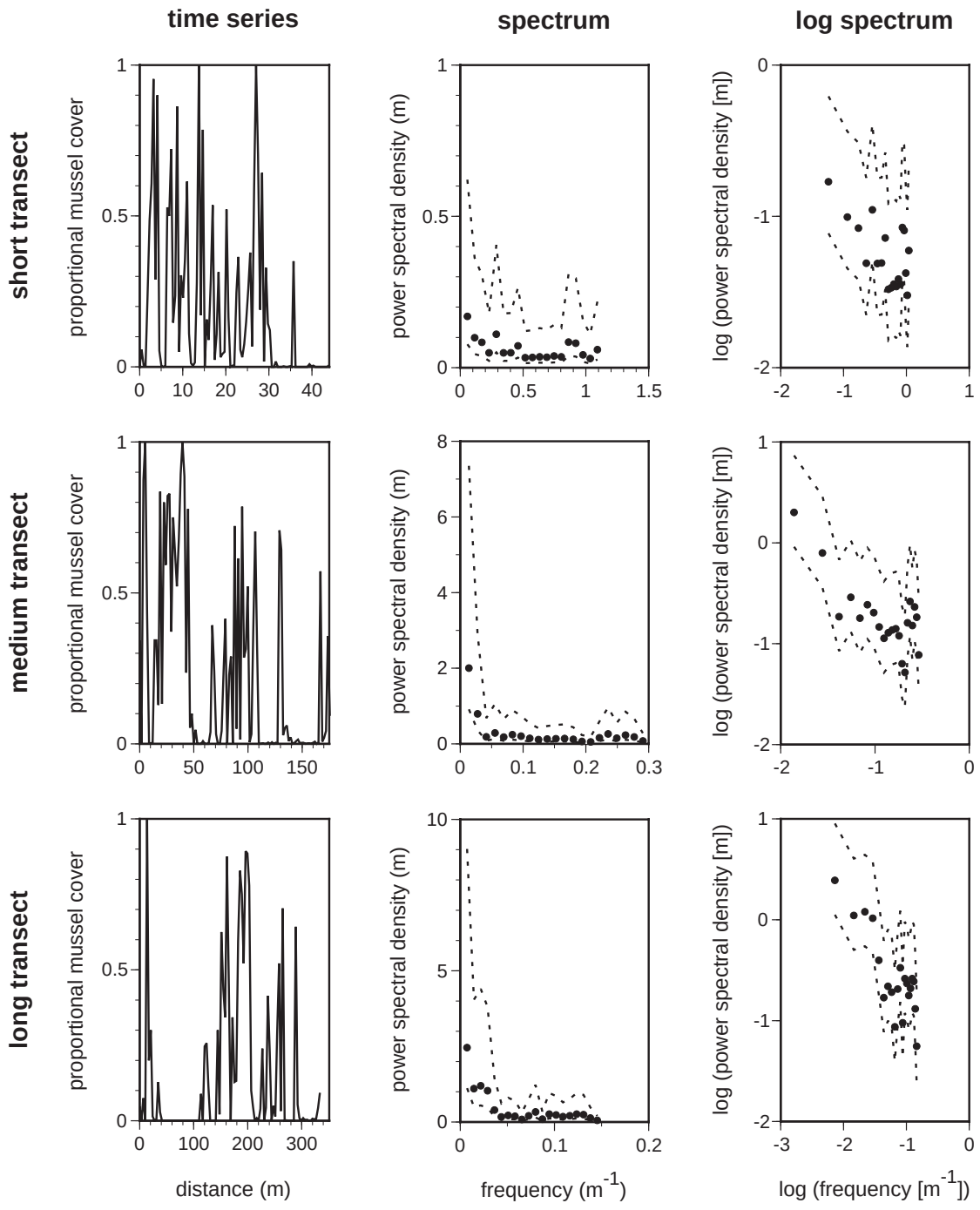
time series
spectrum
log spectrum
short transect
medium transect
long transect
proportional mussel cover
power spectral density (m)
log (power spectral density [m])
distance (m)
frequency (m-1)
log (frequency [m-1])

Fig. E11

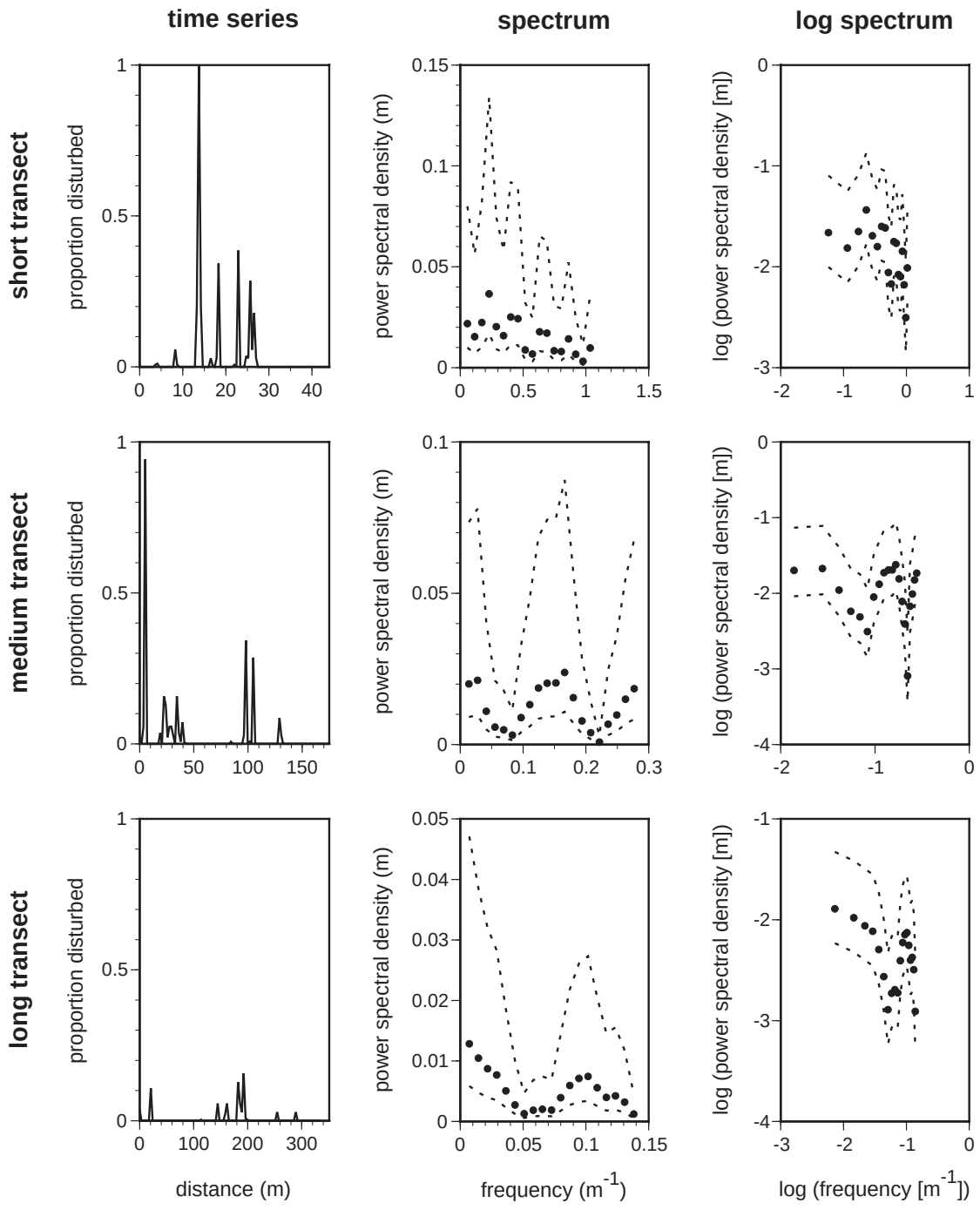
time series
spectrum
log spectrum
short transect
medium transect
long transect
proportion disturbed
power spectral density (m)
log (power spectral density [m])
distance (m)
frequency (m-1)
log (frequency [m-1])

Fig. E12

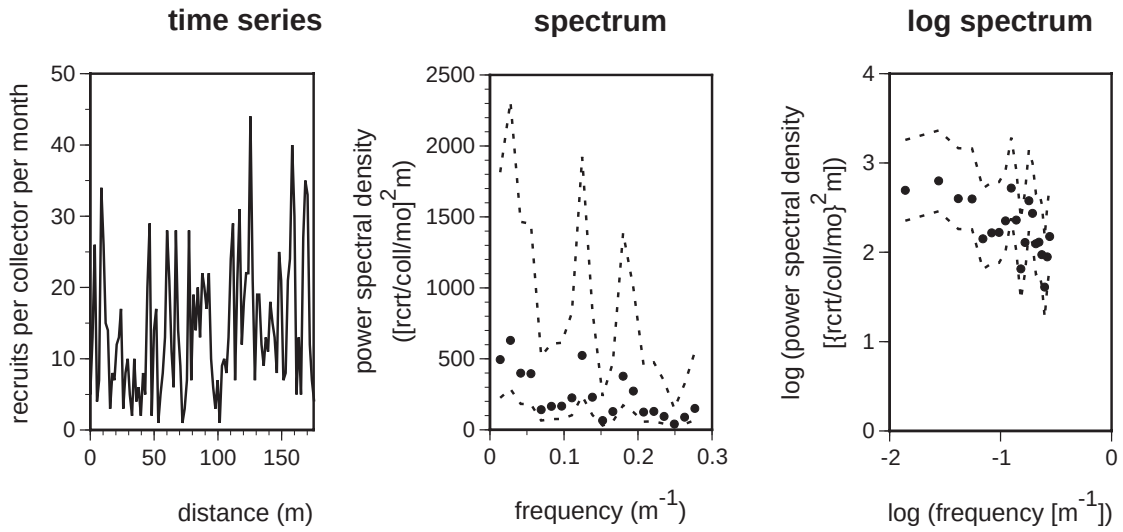
time series
spectrum
log spectrum
recruits per collector per month
distance (m)
power spectral density
([rcrt/coll/mo]2m)
frequency (m-1)
log (power spectral density
[{rcrt/coll/mo}2m])
log (frequency [m-1])

Fig. E13

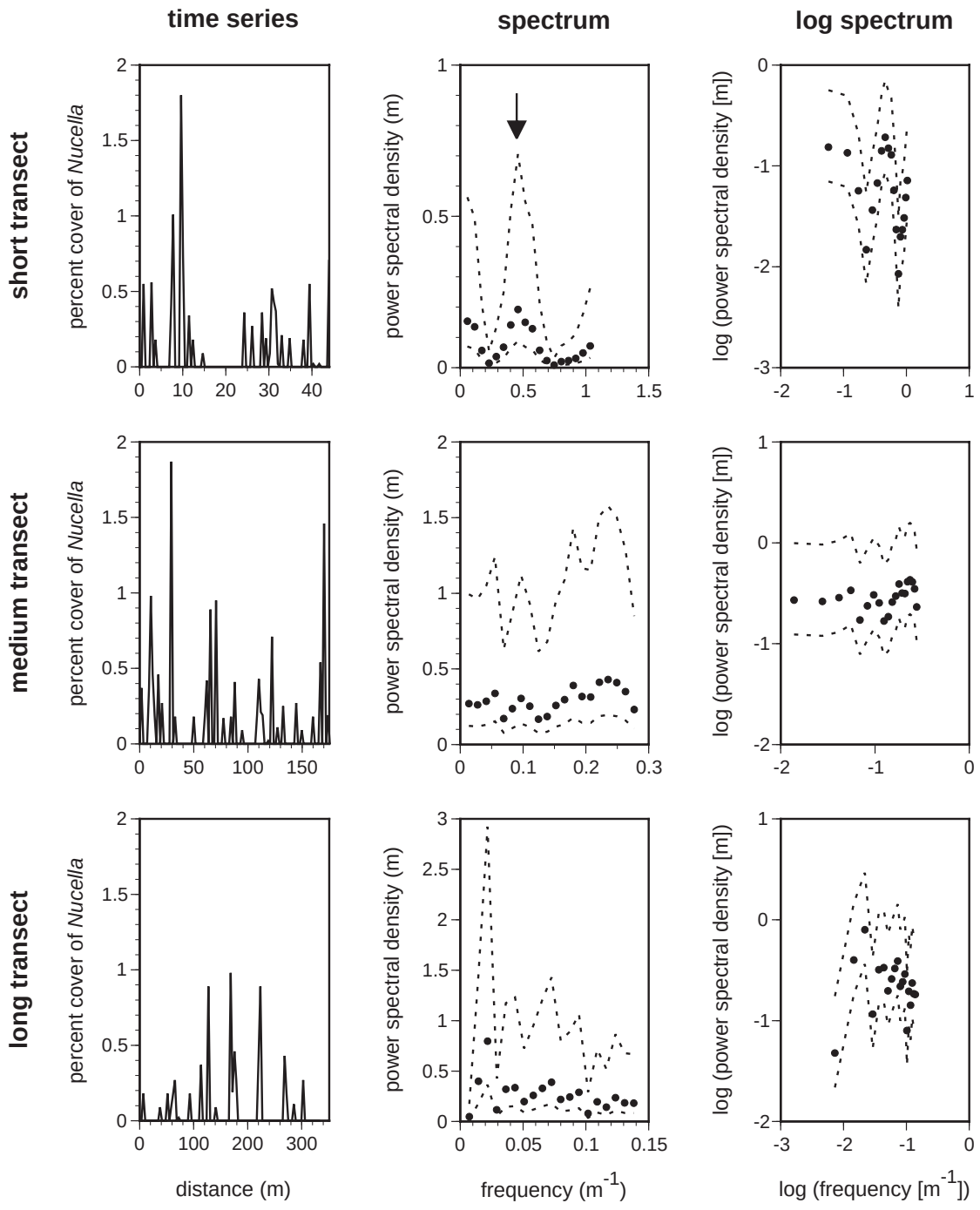
time series
spectrum
log spectrum
short transect
medium transect
long transect
percent cover of Nucella
power spectral density (m)
log (power spectral density [m])
distance (m)
frequency (m-1)
log (frequency [m-1])

Fig. E14

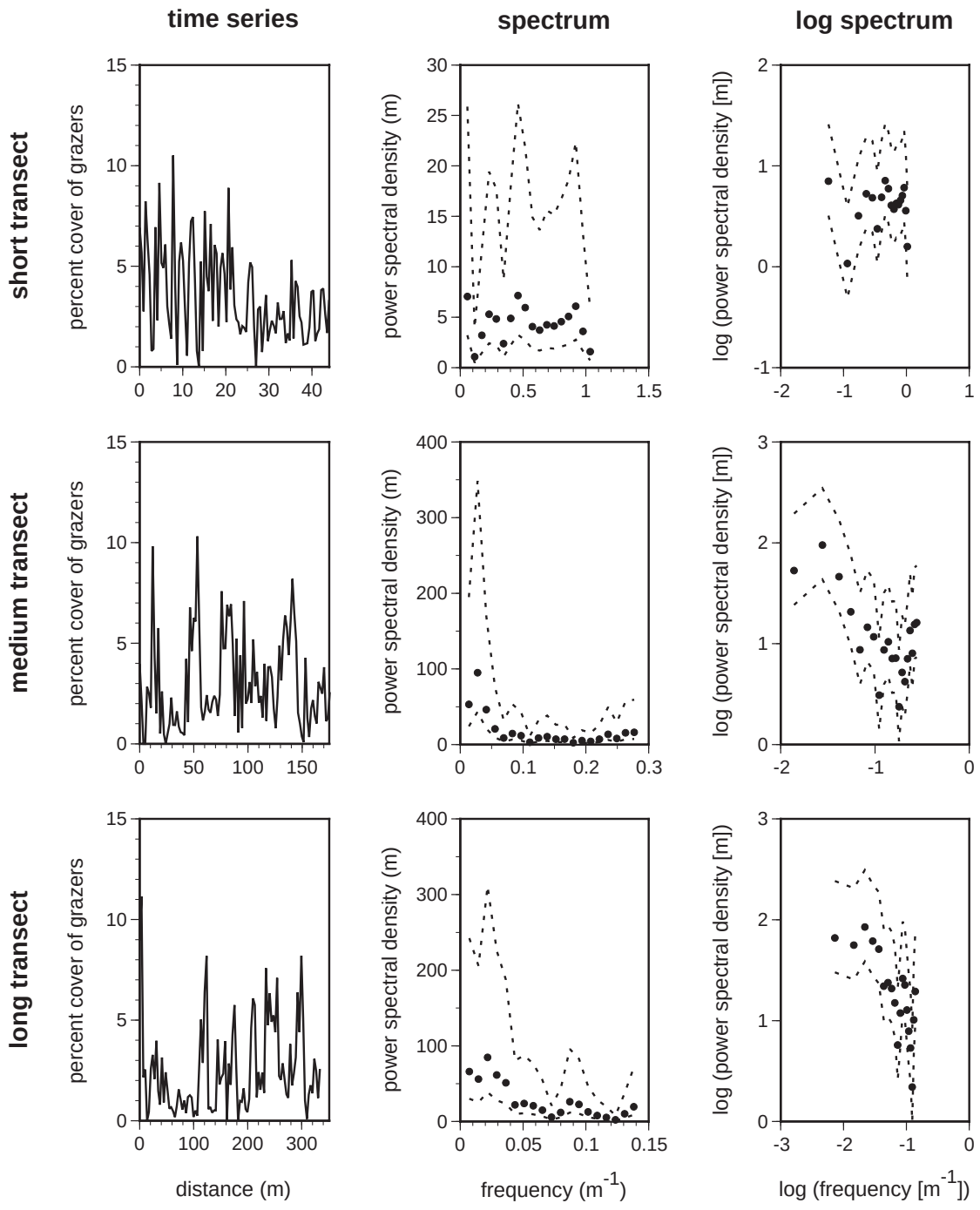
time series
spectrum
log spectrum
short transect
medium transect
long transect
percent cover of grazers
power spectral density (m)
log (power spectral density [m])
distance (m)
frequency (m-1)
log (frequency [m-1])

Fig. E15

Appendix F. 1/*f* Noise, A Review

Because 1/*f* noise is pervasive among our spatial variables, its basic attributes deserve a brief review. β (Eq. 8) typically ranges from 0 to 2. When $\beta = 0$, the autospectral density $S(f)$ is the same at all spatial frequencies. This property is characteristic of processes known collectively as *white noise*. In such a process, the value of a variable at any given location in time or space is independent of (and uncorrelated with) the variable at all other locations. In contrast, when $\beta > 0$, the lower the frequency (that is, the larger the spatial or temporal scale of variation), the larger the variance, and individual measurements are correlated to some extent. One particular case is worthy of note. When $\beta = 1$, the spectrum is known as *pink noise*, and has the property that it is "the natural result of a mixture of different phenomena acting impartially on different scales" (Halley 1996). Although exactly how phenomena interact to yield this type of spectrum remains an area of active research, Halley (1996) makes a compelling argument that pink noise should be considered the null model for environmental and ecological variability.

Pink noise forms an important boundary within 1/*f*-noise processes. For $\beta \geq 1$ and a maximal measurable frequency, f_g, the integral

$$\int_0^{f_g} \frac{\kappa}{f^{\beta}} df = \text{total measurable variance} \qquad \text{(F1)}$$

is improper; it does not converge. In other words, for $\beta \geq 1$, the variance increases without limit as the scale of measurement is increased. This characteristic poses a problem for any definitive measurement of scale. In contrast, if $0 < \beta < 1$, the integral in Eq. F1 does converge. In this case, as the scale of measurement increases, the variance of the process approaches a defined value, and a definitive measure of scale is feasible, although it still may be sensitive to the grain and extent of measurement (see Appendix B).

Literature Cited

Halley, J. M. 1996. Ecology, evolution and 1/*f* noise. Trends in Ecology and Evolution **11**:33-37.

Appendix G. Is There An Alternative to 1/*f* Noise?

Can we be certain that our spectra are indicative of 1/*f* noise? Indeed, spectra with a shape roughly similar to that of 1/*f* noise can result from other models. In particular, it could easily be conceived that the ecological variables we have measured act as first-order autoregressive (AR1) processes. In this case, the value of a variable at one point in space or time depends in part on the value at an adjacent point, as well as on chance. For example, if we follow an autoregressive variable *q* through time:

$$q(t) = \alpha q(t-1) + \varepsilon \qquad \text{(G1)}$$

where $q(t)$ is the value of the variable at time *t*, and $q(t\text{-}1)$ is the value at time t-1. α is the regression coefficient that determines how alike two adjacent points are (on average), and ε is a random variable that can be either positive or negative (Priestley 1981). Autoregressive processes can act in space as well as in time.

The spectra of first-order autoregressive process are in some respects similar to those of 1/*f* noise (Fig. G1). For a portion of the spectrum, the log of the frequency-specific variance decreases approximately linearly with the log of frequency. The most important difference between the spectra of 1/*f* noise and autoregressive processes lies in the low-frequency tail. Whereas a 1/*f*-noise spectrum continues to increase without limit at low frequencies (for any $\beta > 0$), a first-order autoregressive spectrum "flattens out" and both the spectrum and the total variance approach a limit. The definable limit associated with an AR1 process is an appealing alternative to those 1/*f*-noise processes for which $\beta \geq 1$.

The applicability of autoregressive processes is most apparent for temporal data. If the current state of a variable depends at least in part on its state a moment ago, the process is intrinsically autoregressive (although not necessarily to first order). Furthermore, the directional

nature of the autoregressive process described by Eq. G1 is in accord with the nature of time itself. Time's "arrow" ensures that the state of a variable can depend on history, but cannot depend on the future. The application of Eq. G1 to spatial variables is less intuitive, and perhaps less appropriate. The state of a variable at location x might easily depend as much on what is happening at location x+1 as it does on location x-1, but this type of bi-directional dependence is not incorporated in the simple AR1 process described by Eq. G1.

The distinction between 1/f-noise and first-order autoregressive processes disappears under certain circumstances. When α is 1, Eq. G1 describes a random walk, which has a spectrum identical to that of a 1/f-noise process with $\beta = 2$. When α is 0, the result is equivalent to white noise, a 1/f-noise process with $\beta = 0$.

We compared our data (those for which there was no dominant spectral peak) to these two null models (1/f noise, AR1) by calculating on a log-log plot the mean squared error between our spectral estimates and either the best-fit line of a 1/f-noise process or the best-fit curve calculated for a first-order autoregressive process (Priestley 1981). In 18 of the 24 cases, the linear (that is, 1/f) fit yielded a smaller mean-squared error. Three of the six exceptions occurred on the short transect (maximum temperature, species diversity, and mussel disturbance). If these short-transect exceptions are indeed examples of an autoregressive process, the AR1 fit should be even more evident on the medium transect, which, with its greater extent, should reveal more of the flat, low-frequency tail of the spectrum. In each case, however, on the medium transect a linear fit has a lower mean-squared error than does the AR1 fit. In only two cases (species diversity and grazer abundance) does the AR1 process provide the best fit on the long transect.

Given the relatively small number of points in each of our spectra, and the relatively broad confidence limits on each spectral estimate (see Appendix E), it would be difficult to differentiate

definitively between these two null models, but based on this preliminary evidence we proceed on the assumption that the overall spatial variation we have measured is better modeled by a 1/*f*-noise process rather than an autoregressive one. The average β among our variables is 0.69 (*SD* = 0.36). Thus, taken as a whole, our data are "pinkish" noise, in concert with the concepts discussed by Halley (1996), and in general they have a $\beta < 1$, which avoids the problems mentioned above regarding unlimited variance.

Literature Cited

Halley, J. M. 1996. Ecology, evolution and 1/*f* noise. Trends in Ecology and Evolution **11**:33-37.

Priestley, M. B. 1981. Spectral analysis and time series. Academic Press. New York, NY.

Figure Legend

Figure G1. A comparison of the spectra for a 1/*f*-noise process and a first order autoregressive process. The spectra diverge at low frequencies.

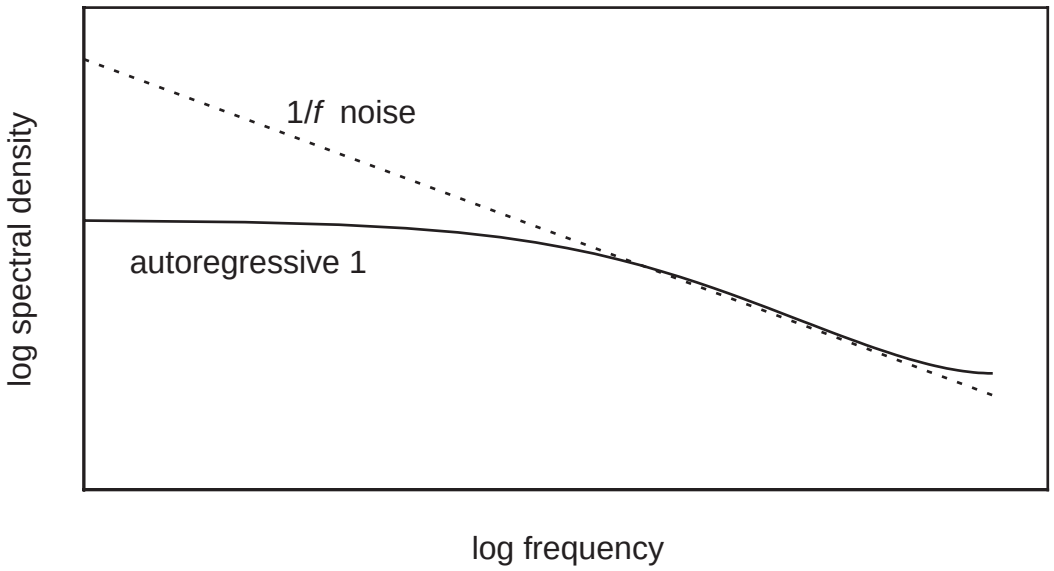
1/f noise
autoregressive 1
log spectral density
log frequency

Fig. G1

Appendix H. Making Measurements in a 1/*f*-Noise Environment

The type of variation exhibited by our spatial variables (the larger the scale of measurement, the larger the associated variance) raises several practical issues, two of which we examine here.

(1) We propose in the text that the measured spectrum of a phenomenon can be used in conjunction with a defined, biological measurement scale to quantify the variance, σ, encompassed by that scale (Fig 8). This approach is particularly useful if there is an inflection point (a "sill") in this curve of σ vs measurement scale (Fig. 3B). Indeed, this inflection point was the basis for defining the variance scale (Eq. 7, B10). One might assume that 1/*f*-noise processes with $\beta \geq 1$ would encounter problems with this approach. If the variance increases without limit as the spatial frequency gets smaller (as it does in this case), won't the standard deviation increase problematically fast as the measurement scale increases, jeopardizing our ability to define the variance scale?

In fact, the situation is not all that bad. Consider, for instance, the spatial pattern of primary productivity, which appears to be a 1/*f*-noise process with a β of 1.36 (Table 3). Despite the inverse relationship between variance and spatial frequency, the standard deviation of maximum force is most sensitive to changes in scale at small scales and a discrete *v*-scale can be discerned (Fig. H1A). The larger β is, the more sensitive the standard deviation becomes to changes in measurement scale at large scales (Fig. H1B), and therefore, the weaker our estimate of the v-scale. But for variables we have encountered ($0 < \beta < 1.5$) this behavior does not pose a serious problem for the estimate of scale.

(2) In this report we have concentrated on measurements of the variation associated with ecological processes and the physical environment. Although variation is undoubtedly important, there are times where it is not the central issue. For example, one might want to explore the effect of

wave exposure on the rate at which snails prey on mussels. Two categories of sites could be chosen in which to measure predation intensity, those on exposed shores, and the others on protected, shores. It would then be traditional to characterize the exposure of each site by measuring some appropriate index (e.g., maximum wave force) at several points within the site, and calculating the mean. Significant differences between the mean exposures of the two categories of sites would validate the assumption that they do, indeed, represent different experimental treatments. However, our ability to discern differences in means is affected by the standard error of the mean (SEM). Given the type of spatial variation found in our study, how are the mean and its standard error affected?

We approach this question by making the following calculation for each of our spatial variables. Each series of data with k number of points was divided into a set of contiguous segments, each of length n (n = 2,3,…k/3). The limit of k/3 is set so that we have at least three segments, as required for the calculations described below. The average value of the data within each segment was computed. These averages were themselves then averaged, and the standard deviation of the averages (by definition, the standard error of the segment mean) was calculated. For each value of n, the extent of the measurement was assumed to be $(n\text{-}1)\Delta x$, where Δx is the spacing between locations (or times) at which the measurements were taken. A plot of the average of averages and the standard error as a function of the extent of measurement then provides the information we seek.

In general, the extent of measurement has little practical effect on the mean itself. In 12 of 25 cases there is a statistically significant trend in the measured value of the mean as a function of extent (9 with a negative slope, 3 with a positive slope), however, the trend is slight (Table H1). In

only two cases is the relative slope (the slope divided by the overall mean) greater than 1%, and on average the relative slope is only 0.3%.

As one might expect, the standard error of the mean decreases with increasing measurement scale (e.g., Fig. H2). However, the autocorrelation of data within each series results in a rate of decrease that is less than one might expect. If data are independent (for instance, if $\beta = 0$), at a given scale of measurement the standard error of the mean varies as $n^{-1/2}$ where n (the number of measurements) is in this case proportional to the extent of the data series. If fact, due to autocorrelation, the standard error decreases more slowly, varying on average ($\pm$ SD) as $n^{-0.334\pm0.175}$ for the spatial variables measured here.

These results suggest that, despite the 1/*f*-noise pattern of variation in our spatial variables, there seems to be no unusual problem in quantifying the mean. As might be expected, the more samples one takes (in this case, implying a larger extent of measurement), the greater the confidence in the resulting average.

We emphasize, however, that the ability to accurately measure a mean and the ability to interpret that mean, may not be the same. For example, on our short transect (with a length of 44 m) the average maximum wave force is 44 N when the offshore significant wave height is 2 m. However, within this short distance the largest force (157 N) exceeds the smallest (15 N) by a factor of greater than 10. Given this large amount of variation in such a short stretch of shore, how useful is the mean maximum force as an index of wave exposure?

Table H1. Scale dependence of the mean. ns = Not significant. Significance level is set at 0.002 (0.05 with a Bonferroni adjustment for multiple comparisons).

		Scale Dependence of the Mean		
	Units	**Mean**	**Slope/Mean**	**Probability**
Force				
short	1/m	41.17	-0.0054	0.000
medium	1/m	42.45	ns	0.048
long	1/m	37.73	ns	0.939
Wave Force Index				
short	1/m	0.575	-0.0032	0.000
medium	1/m	0.551	ns	0.061
long	1/m	0.548	ns	0.016
Temperature				
short	1/m	0.765	ns	0.720
medium	1/m	0.793	0.0022	0.000
Chlorophyll				
medium	1/m	0.976	ns	0.195
Diversity				
short	1/m	0.576	ns	0.101
medium	1/m	0.5898	ns	0.049
long	1/m	0.557	0.000187	0.000
Mussel Density				
short	1/m	0.177	-0.01102	0.000
medium	1/m	0.217	-0.00231	0.000
long	1/m	0.149	ns	0.933
Mussel Disturbance				
short	1/m	0.027	-0.01285	0.000
medium	1/m	0.023	-0.00254	0.000
long	1/m	0.007	-0.0011	0.000
Mussel Recruitment				
medium	1/m	14.51	ns	0.027
Predators				
short	1/m	0.103	ns	0.259
medium	1/m	0.128	-0.00258	0.000
long	1/m	0.067	ns	0.024

Table H1 continued.

Grazers				
short	1/m	3.4	-0.00406	0.000
medium	1/m	3.02	ns	0.003
long	1/m	2.62	0.00068	0.000

Figure Legends

Figure H1. A. Although its $\beta > 1$, the log-log curve of standard deviation versus measurement extent for microalgal productivity exhibits a clear inflection point, thereby allowing the variance scale to be measured. B. Standard deviation as a function of measurement extent for 1/*f*-noise processes with various βs. Unless β approaches 2, it is feasible to use the approximately linear regions of these curves at small and large measurement extent to unambiguously define a variance scale.

Figure H2. The standard error of the mean maximum force decreases with the extent of measurement.

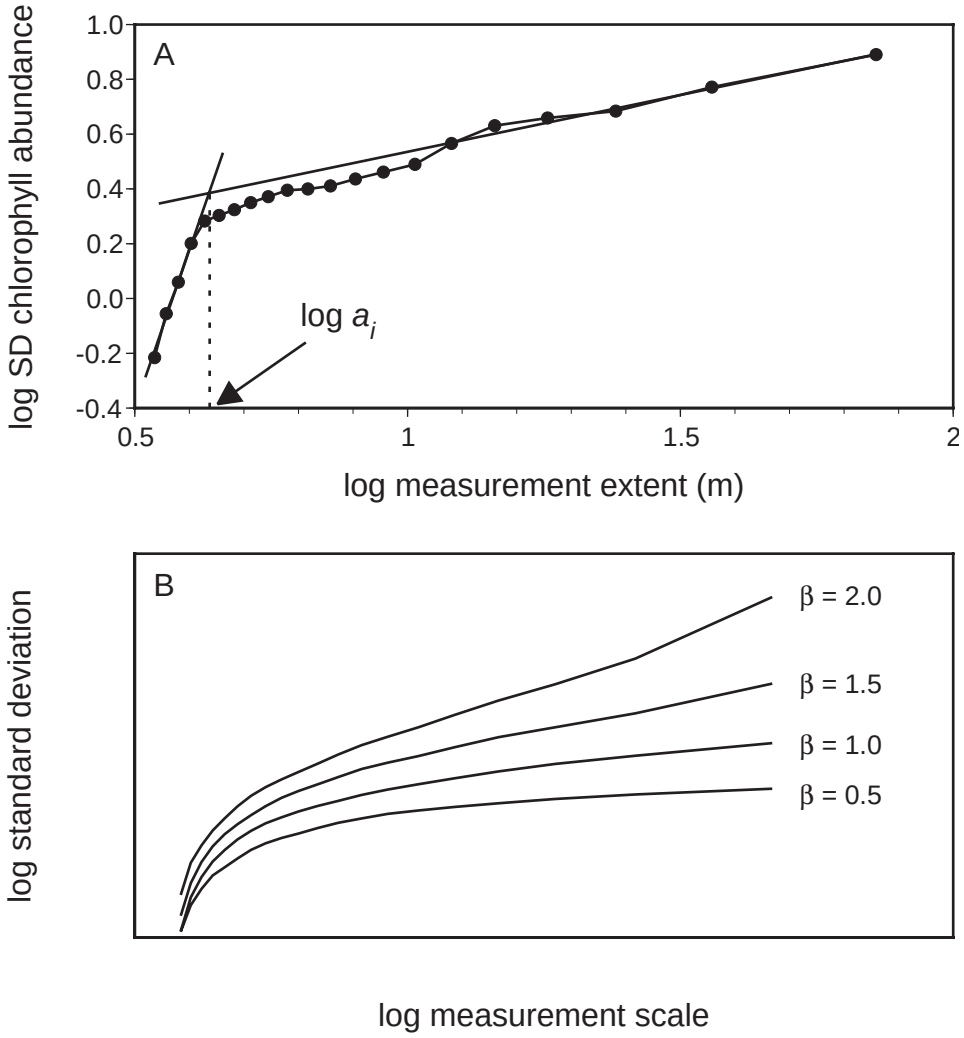
A
log SD chlorophyll abundance
1.0
0.8
0.6
0.4
0.2
0.0
-0.2
-0.4
0.5
1
1.5
2
log a_i
log measurement extent (m)
B
log standard deviation
β = 2.0
β = 1.5
β = 1.0
β = 0.5
log measurement scale

Fig. H1

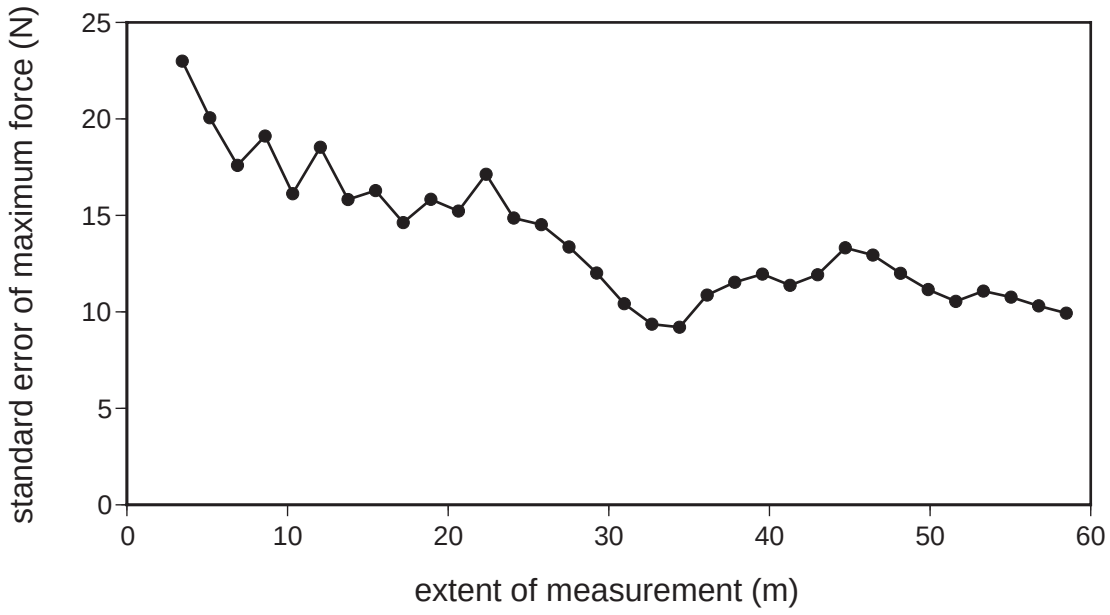
standard error of maximum force (N)
25
20
15
10
5
0
0
10
20
30
40
50
60
extent of measurement (m)

Fig. H2